AD-A068 632 BATTELLE COLUMBUS LABS OHIO F/G 17/1
PRELIMINARY DESIGN STUDY FOR A COMMAND-GUIDED BALLISTIC MISSILE--ETC(U)
OCT 78 G W EWELL, E K REEDY DAAG29-76-D-0100
UNCLASSIFIED DRDMI-T-CR-78-30 NL

| OF |
AD
A068632

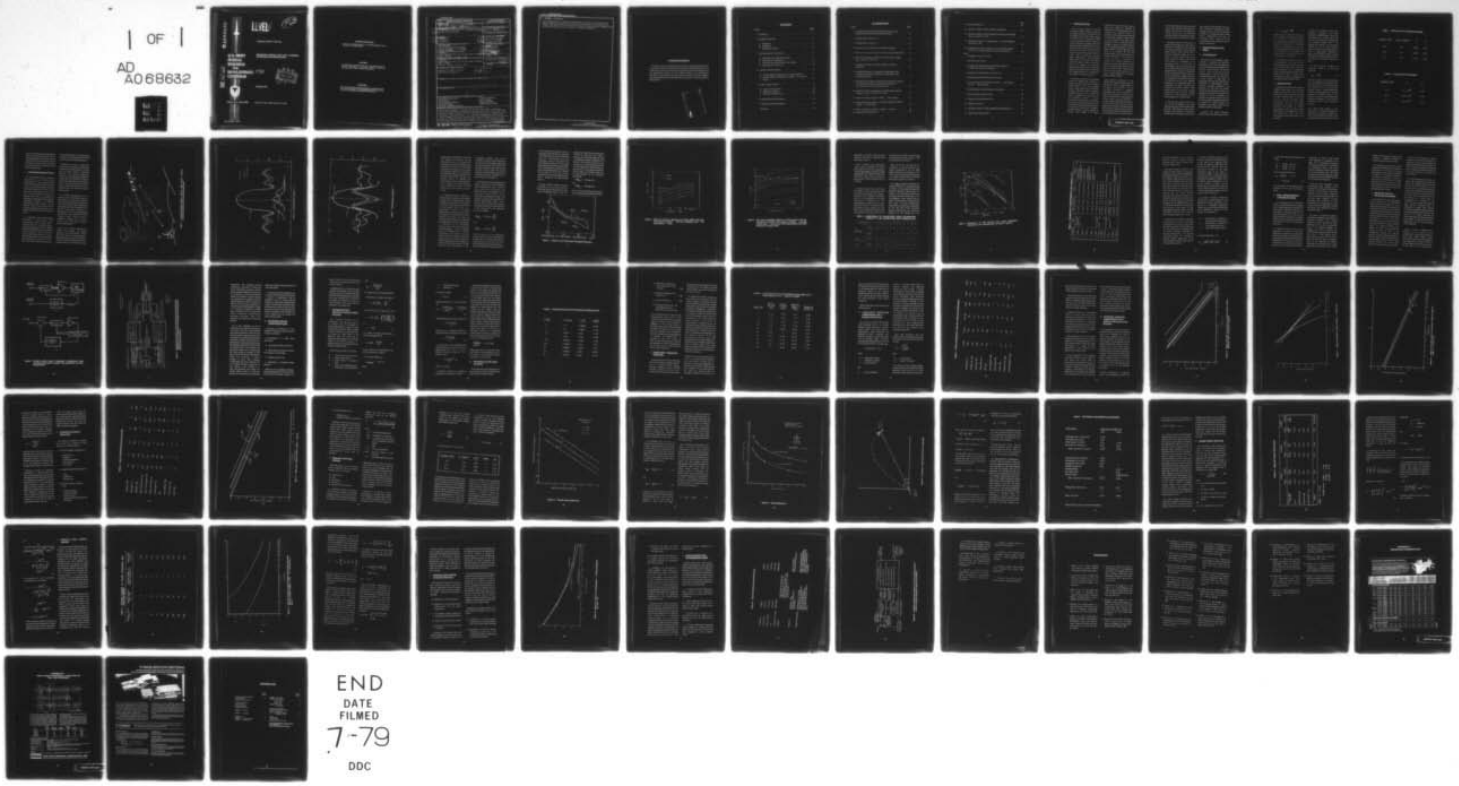

END
DATE
FILMED
7-79
DDC

AD A068632

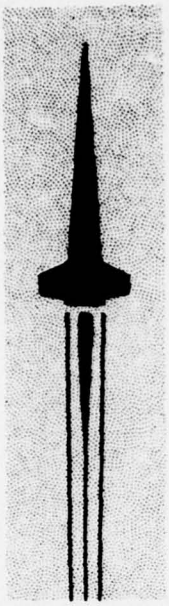

LEVEL II

12

TECHNICAL REPORT T-CR-78-30

U.S. ARMY MISSILE RESEARCH AND DEVELOPMENT COMMAND

PRELIMINARY DESIGN STUDY FOR A COMMAND-GUIDED BALLISTIC MISSILE RADAR

G. W. Ewell
E. K. Reedy

DDC FILE COPY

DDC
RECEIVED
MAY 16 1979
C

18 October 1978

Redstone Arsenal, Alabama 35809

Approved for public release; distribution unlimited.

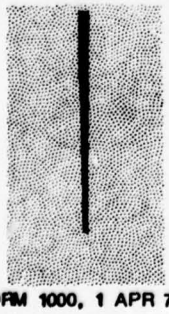

DMI FORM 1000, 1 APR 77

DISPOSITION INSTRUCTIONS

DESTROY THIS REPORT WHEN IT IS NO LONGER NEEDED. DO NOT RETURN IT TO THE ORIGINATOR.

DISCLAIMER

THE FINDINGS IN THIS REPORT ARE NOT TO BE CONSTRUED AS AN OFFICIAL DEPARTMENT OF THE ARMY POSITION UNLESS SO DESIGNATED BY OTHER AUTHORIZED DOCUMENTS.

TRADE NAMES

USE OF TRADE NAMES OR MANUFACTURERS IN THIS REPORT DOES NOT CONSTITUTE AN OFFICIAL ENDORSEMENT OR APPROVAL OF THE USE OF SUCH COMMERCIAL HARDWARE OR SOFTWARE.

UNCLASSIFIED

SECURITY CLASSIFICATION OF THIS PAGE (When Data Entered)

REPORT DOCUMENTATION PAGE

READ INSTRUCTIONS BEFORE COMPLETING FORM

1. REPORT NUMBER: T-CR-78-30
2. GOVT ACCESSION NO.: DRDMI-T
3. RECIPIENT'S CATALOG NUMBER:

4. TITLE (and Subtitle): Preliminary Design Study for a Command-Guided Ballistic Missile Radar.
5. TYPE OF REPORT & PERIOD COVERED: Technical Report
6. PERFORMING ORG. REPORT NUMBER:

7. AUTHOR(s): G.W. Ewell, E.K. Reedy
8. CONTRACT OR GRANT NUMBER(s): DAAG 29-76-D-0101

9. PERFORMING ORGANIZATION NAME AND ADDRESS: STAFF MEMBERS, Engineering Experiment Station, Georgia Institute of Technology, Atlanta, Georgia
10. PROGRAM ELEMENT, PROJECT, TASK AREA & WORK UNIT NUMBERS: 61101A, 1T161101A 91A 00

11. CONTROLLING OFFICE NAME AND ADDRESS: Commander, US Army Missile Research and Development Command, ATTN: DRDMI-TI, Redstone Arsenal, Alabama 35809
12. REPORT DATE: 18 Oct 1978
13. NUMBER OF PAGES: 71

14. MONITORING AGENCY NAME & ADDRESS (if different from Controlling Office): Commander, US Army Missile Research and Development Command, ATTN: DRDMI-T, Redstone Arsenal, Alabama 35809
15. SECURITY CLASS. (of this report): Unclassified
15a. DECLASSIFICATION/DOWNGRADING SCHEDULE:

16. DISTRIBUTION STATEMENT (of this Report)

Approved for Public Release;
Distribution Unlimited.

17. DISTRIBUTION STATEMENT (of the abstract entered in Block 20, if different from Report)

Source = Battelle Columbus Labs

18. SUPPLEMENTARY NOTES

19. KEY WORDS (Continue on reverse side if necessary and identify by block number)

PROPAGATION DATA BASE
BACKSCATTER
DEPOLARIZATION EFFECTS
ROLL MEASUREMENT
FREQUENCY TRADEOFF ANALYSIS
PASSIVE REFLECTOR
ACTIVE BEACON
ANGULAR TRACKING
RETROREFLECTOR RADAR

20. ABSTRACT (Continue on reverse side if necessary and identify by block number)

The US Army continues to develop essentially free-flight or ballistics rockets for providing counterbattery and area fire. The free-flight rocket can deliver high volumes of TOT fire for the destruction of high-value time sensitive, area-type targets. If a relatively inexpensive guidance and control package could be integrated into the free-flight rocket such that the accuracy of these missiles was increased to the 2.0-2.5 mil range, their effectiveness against hard point targets could be significantly increased.

(Continued)

DD FORM 1 JAN 73 1473 EDITION OF 1 NOV 65 IS OBSOLETE

407 080

UNCLASSIFIED

SECURITY CLASSIFICATION OF THIS PAGE (When Data Entered)

20. ABSTRACT (Continued)

Cont

Such a high-accuracy, command-guided ballistic rocket could replace some general and direct support roles calling for munitions to be delivered on targets with high precision and destructiveness and roles where augumentation fires are delivered in close support of maneuver elements.

ACKNOWLEDGMENT

The authors wish to acknowledge the contributions of several individuals at the US Army Missile Research and Development Command (MIRADCOM) toward the completion of this study. In particular, Mr. James Fagan provided excellent technical and administrative support; Dr. James Wright assisted in the collection and interpretation of backscatter and polarization data; and Messrs. Bill Otto, Ed Miller, and Anthony Blackman provided preliminary information on previous efforts at MIRADCOM.

CONTENTS

ILLUSTRATIONS

1. INTRODUCTION

The US Army continues to develop essentially free-flight or ballistic rockets for providing counterbattery and area fire. The free-flight rocket can deliver high volumes of TOT fire for the destruction of high-value, time sensitive, area-type targets. If a relatively inexpensive guidance and control package could be integrated into the free-flight rocket such that the accuracy of these missiles was increased to the 2.0-2.5 mil range, their effectiveness against hard point targets could be significantly increased. Such a high-accuracy, command-guided ballistic rocket could replace some general and direct support cannon and artillery units in fire support roles calling for munitions to be delivered on targets with high precision and destructiveness and roles where augumentation fires are delivered in close support of maneuver elements.

An in-house research and development program at MIRADCOM resulted in a concept for a relatively low-cost, command-guided ballistic rocket with projected accuracy significantly better than the best accuracies obtainable with the completely free-flight rocket [1]. In this concept, the missile is equipped with a receiver, a low-cost guidance package, a unique polarization sensitive passive retroreflector to provide roll position information, and side thrusters to allow the ballistic trajectory to be corrected to agree with a computer-generated reference trajectory designed to produce rocket impact at the target location. In the general concept, a ground-based laser radar was employed to determine rocket spatial position and roll orientation as a function of time. The position and roll data are processed through a ground-based computer which predicts the rocket trajectory and impact point, compares this with a reference trajectory designed to impact at the target location, and then generates trajectory correction signals which are coded on the laser radar beam or an auxiliary RF link and transmitted back to the missile receiver and guidance control units. In this manner, the rocket's trajectory is continuously compared to a reference trajectory and trajectory corrections are made to force the rocket's predicted impact point to agree with the target location, thereby greatly increasing impact point accuracy. This system is called GROWLAR for Guided Rocket With Laser Radar.

The primary limitation of the GROWLAR concept is weather and cloud attenuation of the laser radar signal. To circumvent this problem, a more conventional microwave or millimeter wavelength radar has been proposed to replace the laser tracker. In this case, the radar would perform the same function as the laser tracker previously described — provide position and roll data as a function of time on the missile over the trajectory flight path. The missile retroreflector might take the form of a passive Van Atta array of antenna elements which would be located in the trailing edge of one of the missile fins, or

PRECEDING PAGE BLANK

an active radio frequency transponder could be used. The missile antenna would linearly polarize the returned, retransmitted or reflected signal so that roll orientation processing could be accomplished in exactly the same manner as with the laser tracker.

The primary objective of this study is to determine the feasibility of a microwave or millimeter wavelength radar for satisfying the tracker requirements in the command-guided ballistic missile concept and to develop a preliminary design for such a radar if it proves feasible. Some of the specific tasks which will be a part of this study include (1) examination of the propagation effects on polarization of electromagnetic signals so that the various factors which produce depolarization can be identified and the accuracy of roll position estimation can be determined; (2) analysis of various retroreflector configurations and their polarization and signature properties in comparison with the radar signature properties of the unaugmented rocket; (3) development of several tracking radar candidates and tradeoff analysis of these systems based on such factors as range performance, clutter rejection, tracking accuracy, cost, and complexity; and (4) recommendation of a suitable radar.

In the following sections of this report, the necessary propagation and target reflectivity data base will be developed and described, depolarization effects will be identified and quantified, retroreflector configurations will be analyzed, and various radar systems will be specified. After this, their performance characteristics (range, tracking accuracy, etc.) will be calculated compared. A recommended radar tracking system configuration will then be developed. Major conclusions and recommendations are presented in the last section of this report.

2. PROPAGATION DATA BASE

A. ATTENUATION

Attenuation of electromagnetic signals, especially at microwave and millimeter wavelengths, by the "clear" atmosphere and by rain is an important system parameter for terrestrial target detection and tracking radars, point-to-point ground communication and earth-to-space communications systems. As a basic result of these interests, a large body of experimental data has been assembled on attenuation of electromagnetic signals; numerous theoretical calculations and predictions of atmospheric and weather attenuation have also been developed. The resulting data base has been analyzed and modeled by several researchers with somewhat varying results. In this section, an attenuation model will be defined which will be suitable for tradeoff analysis and prediction of performance for the various candidate missile tracking radars.

A general, and almost universally accepted, attenuation model is given below.

$$A = A_{clear} + MR^N \qquad (1)$$

In this equation, A represents the one-way total atmospheric attenuation in dB/km; A_{clear} is the "clear air" attenuation and R is the nominal rainfall in millimeters per hour (mm/hr). The parameter N is generally treated as a weak function of frequency and sometimes of temperature and polarization. The coefficient M is a strong function of frequency but is a relatively weak function of temperature and polarization.

The attenuation model given in *Table 1* was generated from conservative experimental data given in References 2 and 3 and generally agrees with attenuation models developed for radar propagation analysis and performance prediction. The model given in *Table 1* will be used in subsequent performance calculations for the candidate missile tracking radars.

B. BACKSCATTER

In addition to attenuating microwave and millimeter radar signals, rain also reflects significant energy to the radar. This rain "backscatter" competes and interferes with the target reflected signal in the radar receiver, thereby limiting target detectability and the radar range performance. Therefore, a complete specification and analysis of a radar's performance in adverse weather requires modeling of the rain backscatter in order that target-to-rain clutter ratios and resulting radar range performance can be calculated.

Quality data relating to radar rain backscatter, especially at the higher microwave and millimeter frequencies, are considerably more limited than data relating to attenuation by rain. Perhaps the best currently available data at the frequencies of interest in this study were obtained by the US Army's Ballistic Research Laboratory and Georgia Tech in a series of measurements conducted at McCoy Air Force Base, Florida, in August and September, 1973 [2,4]. These data form the basis for the backscatter model given below.

The most generally accepted rain backscatter model is the following expression:

$$B_V = CR^D, \qquad (2)$$

where B_V represents the rain backscatter cross section per unit volume in M^2/M^3, and R is again the rain rate in millimeters per hour (mm/hr); D is an exponential parameter which is weakly dependent on frequency, while the parameter C is strongly dependent on frequency. Values for the parameters C and D were derived from data presented in References 2 and 4 and are presented in *Table 2* as a function of frequency.

No explicit data relating to rain backscatter at 16 GHz were presented in these references; therefore, the values for C and D at 16 GHz given in *Table 2* were interpolated from the 10 GHz and 35 GHz

TABLE 1. PROPAGATION ATTENUATION MODEL

Frequency (GHz)	A_{clear} (dB/km)	M	N
10.0	0.02	0.0087	1.144
16.0	0.05	0.039	1.124
35.0	0.13	0.239	1.034

TABLE 2. RAIN BACKSCATTER MODEL

Frequency (GHz)	C	D
9.4	1.3×10^{-8}	1.70
16.0	8.52×10^{-8}	1.70
35.0	1.25×10^{-6}	1.71

values by assuming that B_v is dependent on frequency raised to the fourth power (B_v-f^4). The resulting model given in *Table 2* for rain backscatter will be used in later sections of this report to estimate levels of rain clutter and determine MTI requirements for the missile tracking radar.

C. DEPOLARIZATION EFFECTS

The sketch shown in *Figure 1* illustrates the primary factors which produce depolarization of the transmitted radar signal. The antenna and associated radome (1), the intervening propagation medium, both clear air and adverse weather (2), and the target scattering characteristics (3) are the primary polarization-determining elements which must be considered in developing a system design which includes a polarization technique for indicating instantaneous missile rotational or roll position. Each of these factors will be discussed individually and bounds on the depolarization factors will be derived in this section.

(1) ANTENNA AND ASSOCIATED RADOME. A well-designed and manufactured reflector antenna with a horn-type feed can be expected to achieve polarization isolations of between 35 dB and 45 dB, with 40 dB being a realistic, nominal value [5-8]. *Figures 2* and *3* illustrate the antenna performance achieved in an X-band parabolic reflector antenna designed and developed by Georgia Tech for a polarization diversity processing radar [9]. As seen in these figures, on-axis polarization isolation for this antenna exceeds 35 dB in both the elevation and azimuth planes.

Although the on-axis polarization isolation of this antenna is relatively high, moving off the principal planes or into the side lobe region results in a significant decrease in the antenna polarization isolation. For this antenna, the polarization isolation decreases to between -17 dB and -20 dB at the 3 dB points of the main beam. This is a general characteristic of reflector antennas. Polarization isolation is worst in the planes which are rotated 45° from the principal planes.

To minimize depolarization of an antenna in the case of off-axis reception or transmission, it is essential that a primary feed having good polarization isolation be used. Several primary feeds satisfying this requirement have been developed [10-12]. Off-axis polarization properties of Cassegrainian and front-fed paraboloidal antennas have been considered in several references [13-16]. Where necessary, cancellation techniques can be used to achieve cross polarization isolation approaching 60 dB [17].

Water on the antenna, especially the primary feed aperture, can produce significant cross polarizations [18-21]. Worst-case values for cross polarization in these antennas varies between -13 dB and -5 dB when the primary feed aperture is wet as compared with a dry or clear weather value

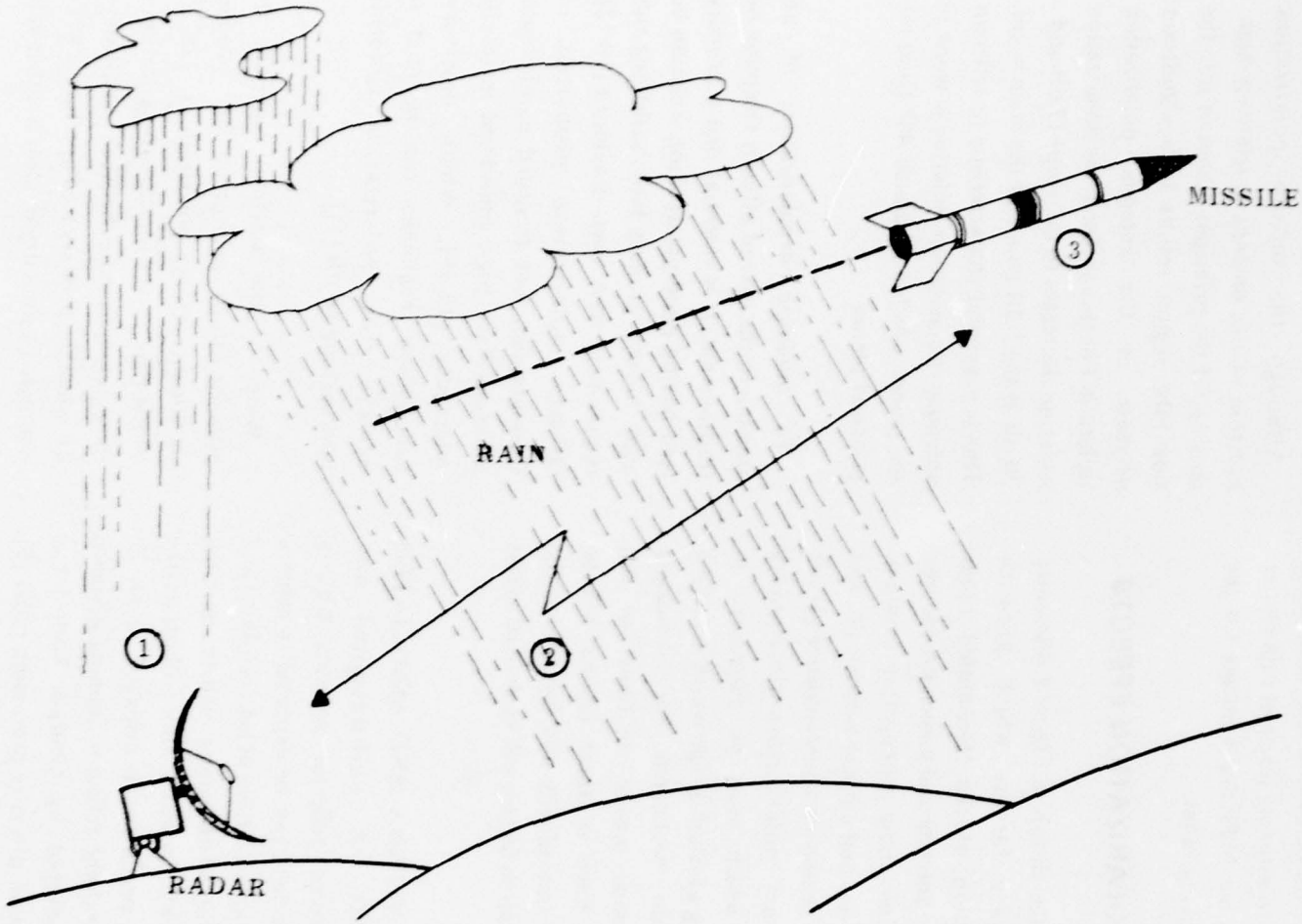

Figure 1. Command-guided ballistic missile radar system concept illustrating components producing depolarization.

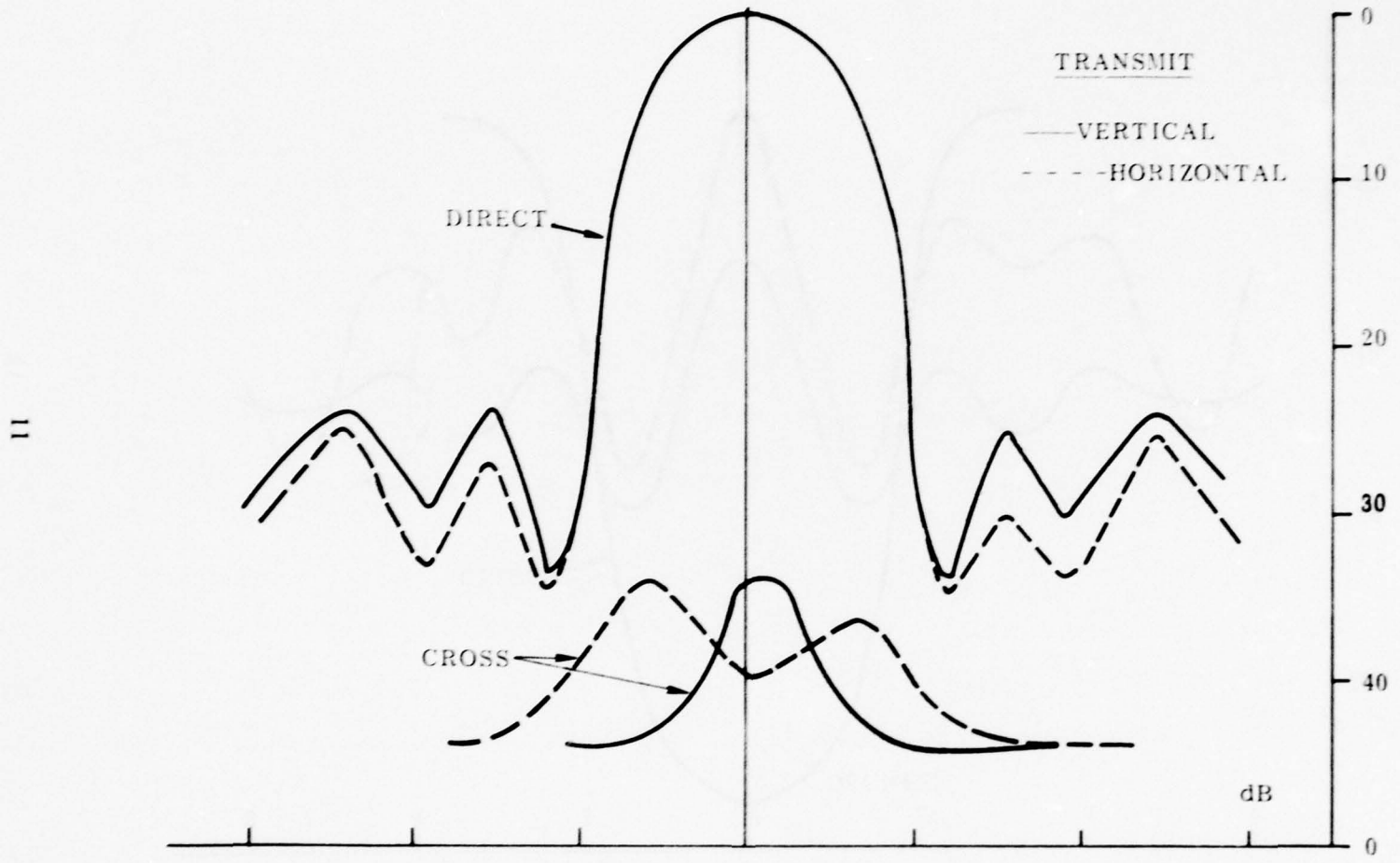

Figure 2. Azimuth pattern; elevation = 0°.

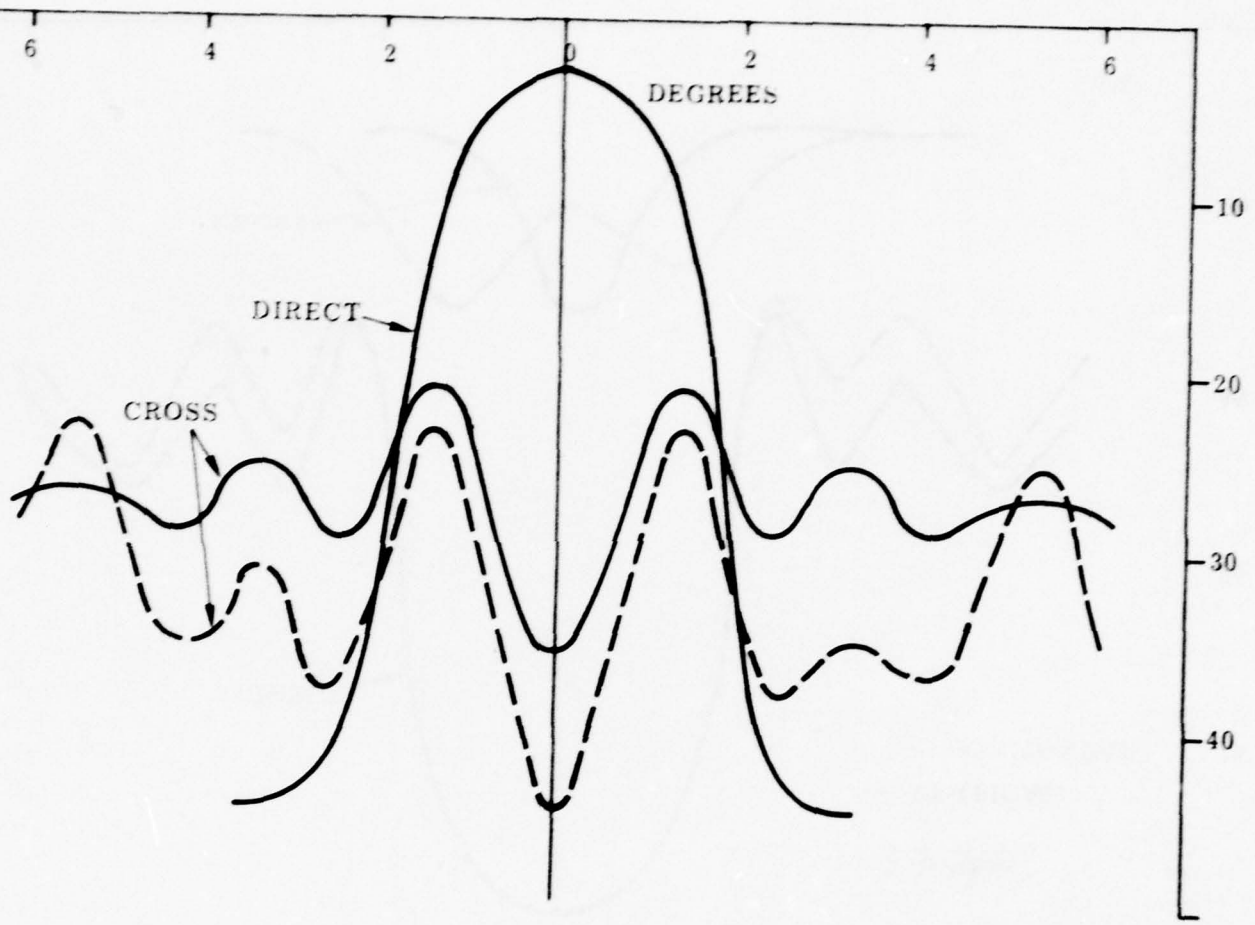

Figure 3. Azimuth pattern; elevation = 1°.

of approximately 40 dB. Snow on antenna feed apertures and radomes can also significantly lower cross-polarization discrimination [18,19,22]. Propagation tests conducted at 19.0 GHz over a 4.1 km path showed that cross polarization was reduced to 24 dB when radomes were covered with snow. Heated radomes are typically used to circumvent this problem. Radomes are obviously effective in reducing cross polarization from rain also. Spraying water on the radome of an antenna having a nominal polarization isolation of 40 dB resulted in an isolation reduction of only 1 to 2 dB.

(2) PROPAGATION MEDIUM. Depolarization introduced by the medium through which an electromagnetic signal propagates can normally be attributed to either clear weather depolarization effects or rain-induced (hail, snow, etc.) depolarization. Causes of clear weather depolarization are primarily the off-axis characteristics of the transmit and receive antennas (previously discussed), ray bending due to bulk refraction, or multipath propagation due to either ground reflections or stratification of the tropospheric refractive index. Since the radar tracking, command-guidance system considered herein will normally track at elevation angles above 4° and, therefore, in normal operation will never experience main beam ground intercept, ground-reflection-induced depolarization can be neglected. In addition, depolarization produced by bulk refraction and stratification of the tropospheric refractive index will be considered small and will be neglected. It may be necessary to investigate and quantify these effects somewhat more exactly at some later time during the system definition and evaluation phase should they become important. Thus, the primary contributor to propagation-induced depolarization is adverse weather, normally rain.

Depolarization by canted raindrops is the largest contributor to total propagation-induced depolarization and is a result of both differential attenuation and differential phase shift between the two orthogonal polarizations. Cross-polarization discrimination (XPD) is the parameter normally used to quantify rain-induced depolarization effects and is defined as the ratio of the power received in the principal polarization channel (parallel) to that converted into the orthogonal polarization channel.

$$XPD_{HV} = 20 \log \left| \frac{\Delta E_V}{E_H} \right|$$

and

$$XPD_{VH} = 20 \log \left| \frac{\Delta E_H}{E_V} \right|$$

where E_H and E_V are the co-polarized received field (the same as transmitted or parallel), ΔE_H is the cross polarized field transferred from E_V, and ΔE_V is the cross polarized field transferred from E_H. Because the rain attenuation for vertical polarization

is less than that of horizontal, the cross-polarization discrimination for transmitted vertical polarization is expected to be better than for transmitting horizontal polarization. *Figure 4* [5] confirms this point. Measured values for XPD_{VH} average approximately 2 to 4 dB better than XPD_{HV} for a fixed attenuation. In addition, theory predicts and measurements have confirmed [5] that both 45° linear and circularly polarized waves suffer severe depolarization effects — perhaps 10 to 12 dB worse than vertical.

In *Figure 5*, XPD is shown as a function of frequency for various values of rain rate. The average raindrop canting angle is 5 deg. and the propagation path is 1 km. This figure shows that XPD has a maximum at 30 GHz for high rain rates. *Figure 6* illustrates the relationship between XPD and propagation distance computed at 19.3 GHz for various values of rain rate. From this figure, it is evident that XPD, especially in vertical polarization, tends to saturate for high rain rates as the propagation distance becomes longer. The saturation values can be approximated by the following relationships:

$$XPD_{HV} = 20 \log \cot \phi$$

and

$$XPD_{VH} = 20 \log \tan \phi$$

where ϕ is the average drop canting angle. For a canting angle of 5 deg XPD saturation

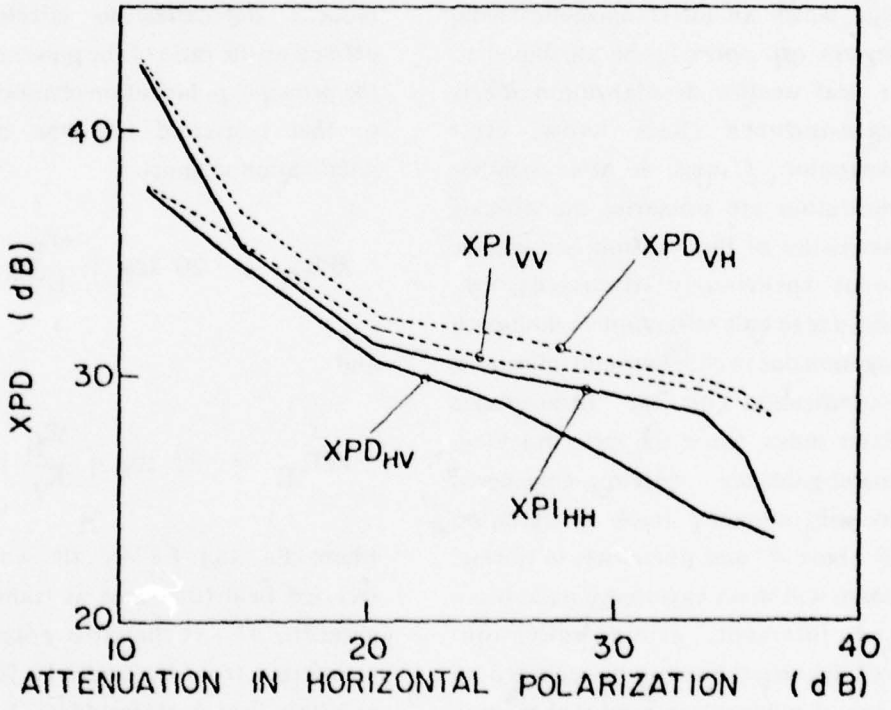

Figure 4. Variation of four XPD values with signal attenuation.

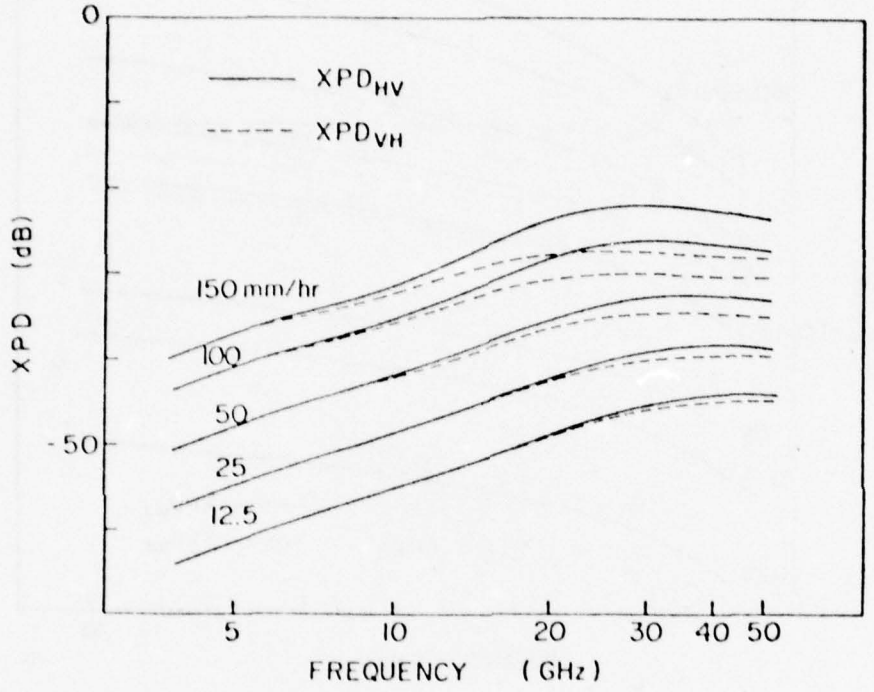

Figure 5. XPD as a function of frequency for various values of rain rate. (The angle of incidence is 90 deg.; propagation path = 1 km; canting angle = 5 deg.)

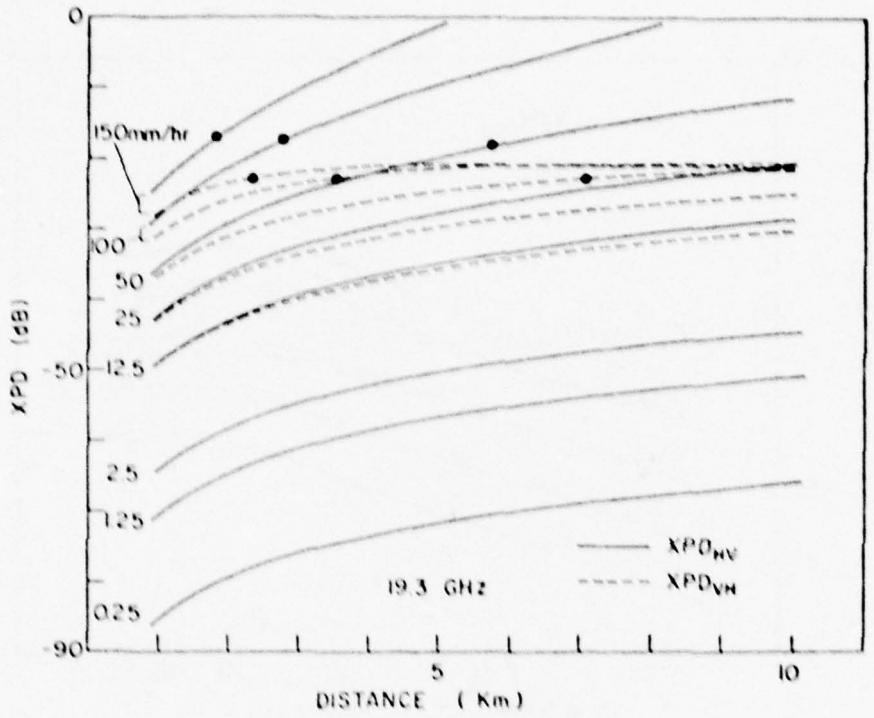

Figure 6. XPD versus propagation distance for various values of rain rate, calculated at 19.3 GHZ. (The angle of incidence is 90 deg. Canting angle = 5 deg. Dots on curves show distance over which attenuation exceeds 30 dB.)

approaches -21.16 dB as given by these equations. This value is confirmed by the data given in *Figure 6*.

Table 3 compares cross polarization values (XPD_{VH}) calculated by various researchers at 11 GHz over a 1 km path for a 15 deg canting angle and various rain rates ranging from 1.25 to 100 mm/hr [23]. Cross polarization values tend to saturate at approximately -25 dB to 26 dB for this set of conditions.

Long-term measurements of XPD have been made in various countries for both terrestrial and earth-space links. *Figure 7* summarizes the cumulative distribution statistics of XPD gathered from recent publications. Parameters of the measurements are listed in *Table 4*. Close inspection of these curves indicates that the polarization isolation between the two linearly polarized channels exceeds -25 dB approximately 99 percent of the time for frequencies in the 10 GHz to 35 GHz range; the polarization isolation exceeds -33 dB almost 90 percent of the time.

Based on the data reviewed above, a conservative or worst-case value for rain-induced depolarization over the paths lengths (20-40 km) and frequencies (5-18 GHz) of interest in the study will be assumed to be -22 dB to -25 dB, with the transmitted polarization assumed to be vertical.

(3) TARGET INDUCED DEPOLARIZATION EFFECTS. A complicated radar or scatterer, such as a missile, having several physically separated scattering centers or surfaces is very polarization sensitive and will always produce depolarization of the electromagnetic energy scattered from its surface. Unfortunately, very little data have been taken on missile depolarization characteristics in general and, in particular, for the Little John missile. Theoretical analysis of missile radar cross section and prediction of both parallel and cross

TABLE 3. COMPARISON OF CALCULATED CROSS POLARIZATION (XPDVH) AT 11 GHz, AFTER EVANS AND THOMPSON [a3]

RAIN RATE (mm/hr)		1.25	2.5	12.5	25	50	100
CROSS-POLARISATION (LINEAR) (dB) FOR $\theta = 15°$ CANTING ANGLE 1 km path	EVANS/ TROUGHTON	66.02	56.24	42.90	37.51	31.84	26.00
	WATSON/ ARBABI	–	59.16	47.15	37.87	31.82	27.48
	MORRISON/ CHU	65.79	52.91	44.13	37.71	31.23	25.01
	OGUCHI/ HOSOYA	66.74	60.24	45.11	38.64	32.17	25.82

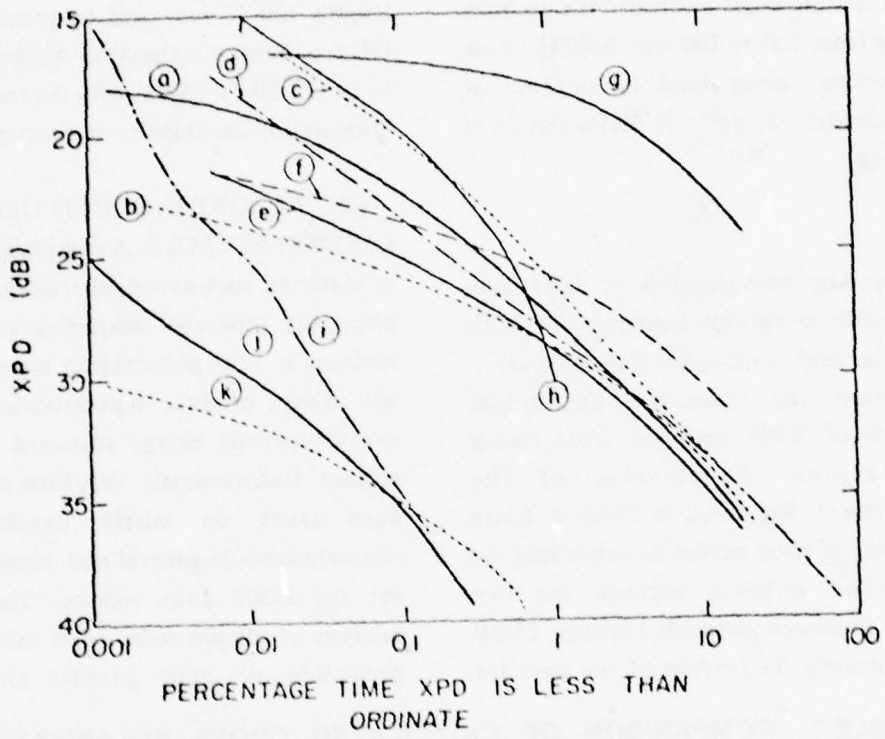

Figure 7. Distributions of XPD gathered from recent publications. (Parameters of the measurements are listed in Table 4.)

TABLE 4. PARAMETERS OF MEASUREMENTS FOR CURVES a TO k

	Polarization	Names	Freq.	Path Length	Period	Remarks
a	XPD_{HV},	Watson, McEwan, Ghobrial, and Arbabi (35)	11 GHz,	13.6 km,	May 1972 to April 1973,	All types of fading. (Curves excluding multipath is negligibly different)
b	XPD_{VH},	" " ,	11 GHz,	13.6 km,	May 1972 to April 1973,	All types of fading.
c	XPD_{VH},	" " ,	11 GHz,	13.6 km	May 1971 to April 1972,	All types of fading. (Except 2 months when horizontal)
d	XPD_{VH},	" " ,	11 GHz,	13.6 km,	May 1971 to April 1972,	Excluding clear weather multipath
e	XPD_{HV},	(29) Watson, McEwan,	11 GHz,	13.6 km,	May 1973 to April 1974,	
f	XPD_{VH},	Turner (37),	22 GHz,	4 km,	Jan. 1972 to May 1972,	
g	XPD_{HV},	" ,	22 GHz,	4 km,	Feb. 1972 to April 1972,	
h	XPD circ.	(44) Inoue & Akiyama,	6.72 GHz,	37.2 km,	Sept. 1971 to Oct. 1971,	Over-sea path
i	XPD	(45) Morita et al,	19.0 GHz, 19.1 GHz,	2.9 km, 4.3 km,	Jan. 1972 to Dec. 1972,	
j	XPD_{HV},	" ,	19.3 GHz,	4 km,	July 1972 to Oct. 1972,	Slant propagation path close to sea shore
k	XPD_{VH},	" ,	19.4 GHz,	4 km,	July 1972 to Oct. 1972,	

polarization signatures is an extremely difficult analytical problem, usually requiring large computer programs and significant machine time.

Some data of limited relevance to the problem of missile (similar to a Little John) depolarization were taken on the BQM-34A and BQM-34F target drones at the US Air Force Radar Target Scattering Division (RAT SCAT), Holloman Air Force Base, New Mexico. Both parallel and cross polarization monostatic and bistatic RCS data were measured at a frequency of 5.5 GHz. Detailed inspection of these data indicates that, for vertical transmit polarization, the reflected monostatic cross polarization component varies between -23 dB and -5 dB with respect to the parallel component for the BQM-34F drone over the 30 deg interval about the tail-on aspect (the interval of most interest for the command-guided missile radar). The mean polarization isolation value over this interval is approximately -8 to -12 dB.

If these data are assumed to be reasonably representative of the scattering characteristics for the missile of interest (this assumption is necessary for the present since no other relevant data are available), then the missile depolarizes sufficiently to preclude high-accuracy roll position measurement based on ε polarization signature without augmentation of the missile backscatter signature and control of its polarization properties.

A passive retroreflector based on a Van Atta array technique is proposed elsewhere in this report as an approach which increases the apparent target RCS and, simultaneously, achieves improved polarization isolation in the signal transmitted back to the radar. A conservative estimate of the polarization isolation which can be achieved with this retroreflector techniques is -19 dB to -25 dB. In addition, active augmentation of the missile signature using a beacon transponder on board the missile and a Van Atta re-radiating antenna array can be used to achieve still larger polarization isolation and target RCS if necessary.

(4) TOTAL SYSTEM DEPOLARIZATION. If we assume that each of the depolarization effects considered in this section is a statistically independent, random process, then total depolarization can be calculated by using a root-sum-square (rss) relationship. If

D_a = depolarization contributed by antenna/radome combination,
D_p = depolarization contributed by the propagation path, and
D_t = target induced depolarization,

the total depolarization, D_s, is

$$D_s = \sqrt{Da^2 + Dp^2 + Dt^2} \qquad (3)$$

For the following assumed depolarization values,

$$D_a = -35\ dB = 3.16 \times 10^{-4}$$
$$D_p = -23\ dB = 5.0 \times 10^{-3}$$
$$D_t = -19\ dB = 1.2 \times 10^{-2},$$

the total system deploration is

$$D_S = \sqrt{169.1} \times 10^{-3}$$
$$= -18.8\ dB \qquad (4)$$

For this example, the total depolarization is dominated by the target depolarization effects.

3. ROLL MEASUREMENT CONSIDERATIONS

A basic requirement for a GROWLAR missile is a knowledge of missile roll angle in order to enable appropriate side thrusters to be actuated to generate required course corrections. The concept considered for roll angle measurement involves the use of a missile-referenced polarization re-radiated by the missile as a means for determining the roll angle of the missile by a ground-based radar sensor.

It is generally desirable to utilize a linear polarization (as opposed to some other polarization, such as circular) re-radiated by the missile as a means of sensing missile roll angle. Such a linearly polarized signal may be generated by either an active beacon-transponder (one containing a microwave source) or by an entirely passive reflector combination. In order to utilize signals whose amplitude is independent of roll angle, use of circular-linear polarization combinations is desirable for the path from the ground-based radar to the missile. Circular polarization could be transmitted by the ground-based radar and linear polarization received at the missile, or linear transmitted by the ground-based radar and circular received by the missile.

There are certain advantages to the ground-based radar radiating circular polarization and the missile receiving linear, primarily in the simplicity of the missile antennas. However, certain complexities are incurred in the ground-based radar. On the other hand, reception of circular polarization and re-radiation of linear polarization by the missile requires a more complex antenna configuration on board the missile, while simplifying the ground-based radar system.

The choice of polarization might be influenced by propagation considerations if significant differences were exhibited among the various polarizations. While differences do exist, they are sufficiently small to be considered negligible. For example, at 11 GHz in 5 mm/hr rain, differential attenuation between horizontal and vertical of 0.011 dB/km and a differential phase shift of 0.517°/km has been reported [24]. While propagation effects of this magnitude can produce appreciable cross polarization for circular polarization (on the order of 10 to 12 dB),

the effects on circularity are relatively small, resulting in negligible modulation in received power as the missile rotates.

The following sections treat several topics concerned with implementing the concept of polarization for missile roll and angle measurement. Topics include a discussion of methods of roll angle measurement, retroreflector configuration, analysis of maximum radar cross section of a missile retroreflector, and consideration of some additional reductions in retroreflector radar cross section which would be incurred when implementing such concepts.

A. METHODS FOR ROLL ANGLE MEASUREMENT

The concept of roll angle measurement being considered for the GROWLAR missile invoives the radiation of a body-fixed linear polarization by the missile and utilization of this polarization information to determine missile roll angle. The signal at the missile is produced in response to signals from a ground-based radar, and a passive retroreflector or an active beacon transponder system may be used to generate the missile-referenced linearly polarized signal. Two possible simplified block diagrams of missile beacon-transponder systems are given in *Figure 8*. The configuration utilizing two antennas permits a choice of different polarizations (such as circular/linear) for reception and re-transmission, while that using a single antenna requires use of the same polarization on reception and transmission.

The use of retroreflectors in general necessitates use of the same polarization on reception; in order to achieve a signal with amplitude substantially independent of roll angle, the reflector should be illuminated with a circularly polarized signal and use the same linear polarization on reception and re-transmission.

At the ground-based radar sensor, the angle of the incident signal is determined and the 180° ambiguity of missile position resolved. The 180° ambiguity of missile position may be resolved by firing a known thruster early in flight and then determining missile roll angle by observing the motion of the missile; once missile position has been determined, it is then relatively straightforward to "remember" or keep track of missile roll angle throughout the flight. Received polarization may be determined in several ways, including (1) observing modulation of signals received by a linearly polarized receiver as the missile rotates, or (2) actually measuring the received polarization using a dual-polarized system. Because of data rate and accuracy requirements, only the second technique will be considered.

Figure 9 shows a simplified block diagram of the antenna/receiver configuration for a dual polarized, ground-based radar which radiates circular polarization while receiving two orthogonal linear polarizations; the ratio of these two orthogonal linear polarizations is a measure of the angle of the received linear

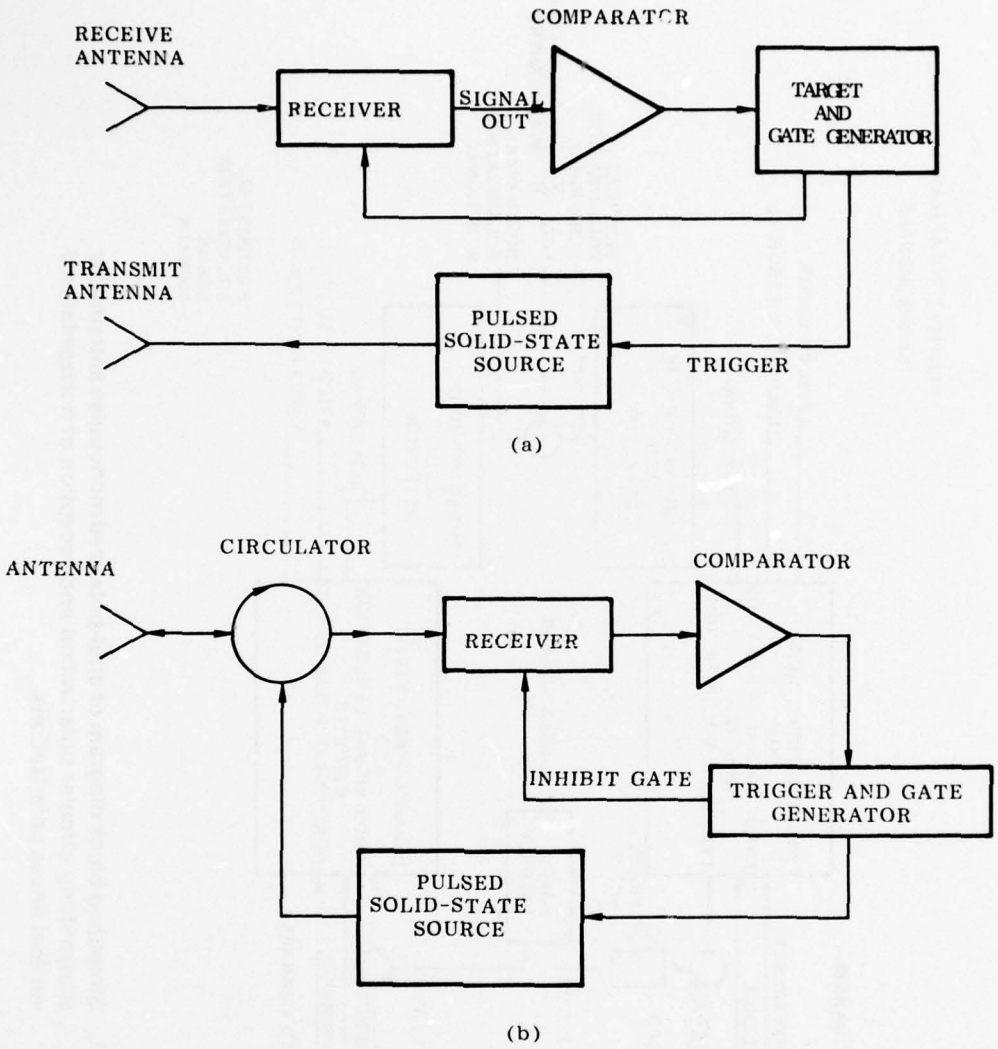

Figure 8. Possible missile beacon transponder configurations using (a) separate antennas for reception and transmission, and (b) a simple antenna.

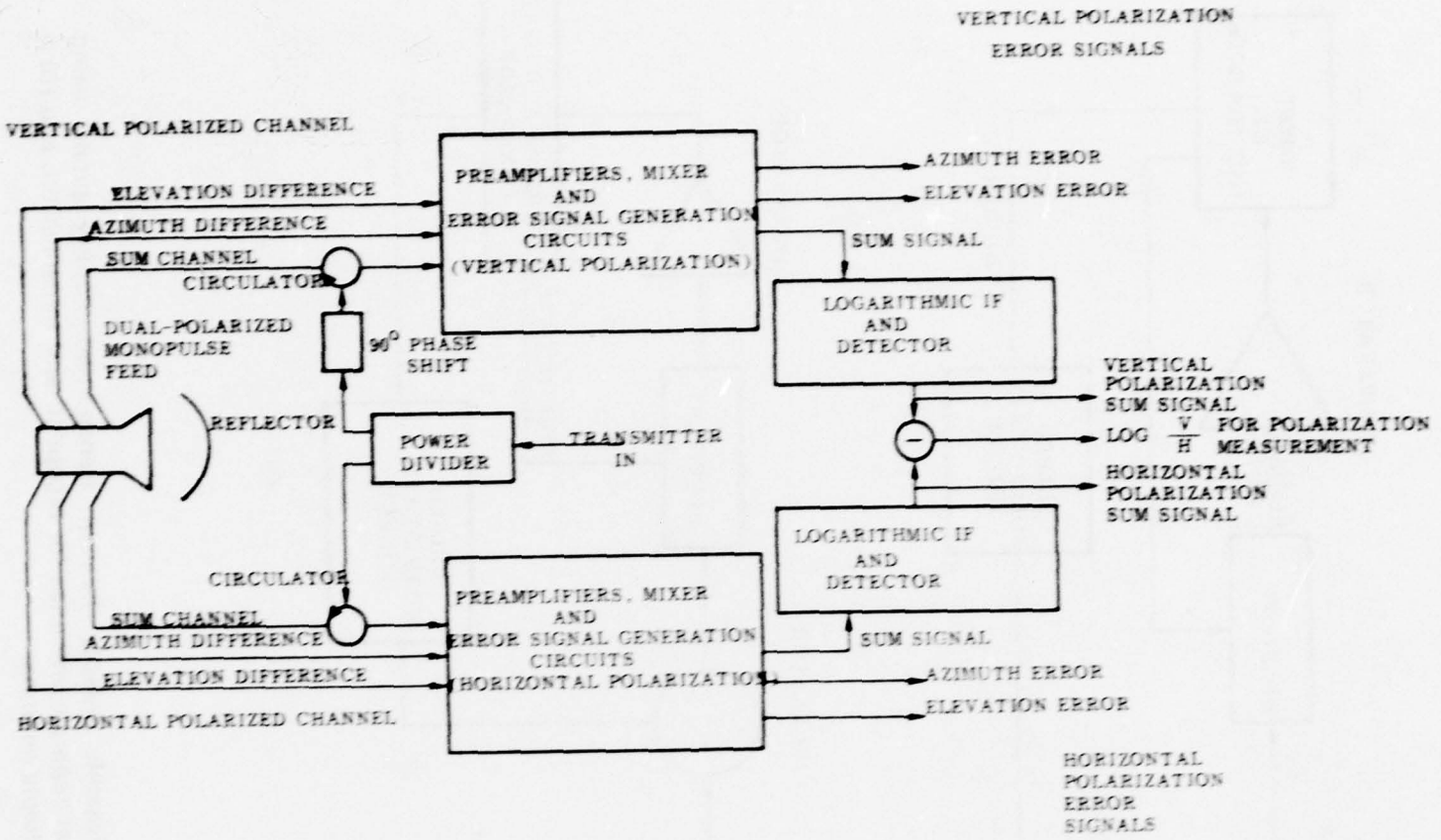

Figure 9. Simplified block diagram of dual-polarized monopulse antenna for transmitting circular polarization and reception of horizontal and vertical linear polarizations.

polarization. The transmitted circular polarization is generated by creating two equal amplitude orthogonal linearly polarized signals differing in time phase by 90°. On reception, the two linearly polarized signals are processed to generate angular error signals and the logarithm of the sum signals subtracted to yield the logarithm of the ratio of the two linear components. All of the devices in the block diagram of *Figure 9* are standard, commercially available items including the power divider, phase shifter, circulators, dual-polarized monopulse antennas, angle track processors, and logarithmic IF amps and detectors.

Two of the components of such a subsystem are less widely known than some of the others. The first is a dual-polarized monopulse feed assembly, and the second is the IF monopulse subsystem to generate the error signals. Dual mode couplers have been developed at Georgia Tech [25] and have been produced commercially by Microwave Development Laboratories (MDL). MDL has combined four of these couplers with appropriate hybrids into a dual-polarized feed. Such devices are available as stock items in the 5.5 GHz and 9.5 GHz frequency bands and technology is readily available to extend these techniques to both higher and lower frequencies. The IF monopulse subsystem to generate the error signals is also available as a stock item generating error signals over dynamic ranges as great as 70 dB and provides for incorporation of an amplitude channel for range tracking and selection of track polarization.

This system can produce the angular error for vertical and for horizontal polarizations, a measure of polarization, and the amplitude of the two linearly polarized channels over greater than a 70 dB dynamic range of received signal. Subsequent signal processing can be used to select the error signal for the larger of received signals for further processing, calculate the angle of the received polarization, and perform the range tracking function.

B. RETROREFLECTOR CONFIGURATIONS

Acceptable retroreflectors for the GROWLAR Missile should have a number of features, including:

- Re-radiation of a single linear polarization
- Large effective radar cross section
- Small variation in radar cross section with changes in viewing angle
- Simplicity and low cost
- Adaptability to irregularly shaped apertures

Reflectors such as dihedrals, trihedrals, spheres and flat plates all fail to have some of these desired properties. However, an

array of the Van Atta type [26] utilizing linearly polarized elements does possess the desired properties.

Simplified theory of the Van Atta array indicates a wide angular range over which the radar cross section remains rather high. When the mutual coupling factors and other more exact considerations are included in the analysis, the variation of radar cross section becomes more extreme but still acceptable for this application.

C. MAXIMUM RETRO-REFLECTOR RADAR CROSS SECTION

The scattering strength of the retroreflector, or its radar cross section, is an essential piece of information in determining feasibility of these roll angle measurement techniques. While a number of factors influence the achievable radar cross section, an upper bound on the achievable radar cross section may be obtained by assuming that all of the energy incident on the reflector aperture is re-radiated with the maximum gain achievable with the available aperture.

If the following quantities are defined,

S_i = power density of incident field
A_i = effective intercept area
S_s = power density of re-radiated field
G_r = gain of the re-radiating antenna in the direction of measurement

then,

$$S_s = \frac{(S_i A_i)(G_r)}{4\pi R^2}$$

at a range R from the scattering element.

The definition of radar cross section is

$$\sigma = 4\pi R^2 \lim_{R \to \infty} \left| \frac{E_s}{E_i} \right|^2 ;$$

for the far field case $\left|\frac{E_s}{E_i}\right|^2$ reduces to $\frac{S_s}{S_i}$. Thus

$$\sigma = 4\pi R^2 \lim_{R \to \infty} \left(\frac{S_i A_i G_r}{4\pi R^2}\right)\left(\frac{1}{S_i}\right)$$

or

$$\sigma = A_i G_r . \qquad (5)$$

G_r is related to the reflector beamwidths in the two principal planes by

$$G_r \text{ (max)} \approx \frac{41,000}{\theta_1 \theta_2} , \qquad (6)$$

where θ_1 and θ_2 are the beamwidths in the two principal planes in degrees.

For constant illumination

$$\theta_{\text{radians}} = 1.02\ \lambda/a$$

where

λ = operating wavelength
a = aperture size

Converting to degrees,

$$\theta \approx 59\ \lambda/a. \qquad (7)$$

Substituting Equations (7) into Equations (6),

$$G_r = \frac{41{,}000\ a_1 a_2}{(59)^2 \lambda^2} = \frac{11.78\ a_1 a_2}{\lambda^2} \qquad (8)$$

Substituting Equation (8) into Equation (5),

$$\sigma = \frac{11.78\ A_i a_1 a_2}{\lambda^2}$$

and if $a_1 a_2$ (as a rectangular aperture) is associated with the scattering area A_s, then

$$\sigma = \frac{11.78\ A_i A_s}{\lambda^2} \qquad (9)$$

Conversations with MIRADCOM personnel indicate an area of the fin of approximately 11 in.^{2} (5 1/2 × 2 in.), or 70.97 cm^2 or 0.0071 m^2. Thus, if $A_i = A_s = 0.0071$ m^2, then

$$\sigma = \frac{5.9 \times 10^{-4}}{\lambda^2}\ m^2$$

where λ is in meters.

A number of values of σ at different frequencies are summarized in *Table 5*.

An important related question is the value of radar cross section of the remaining portion of the missile. By shaping and selection of appropriate geometries, the cross section of the missile (with exception of the exhaust plume and the exhaust opening) can be significantly reduced since only a dominant rear view will be presented to the radar. The worst-case condition is the condition for which burnout has been achieved and the exhaust nozzle and propellant chamber are visible to the radar. In such a situation, complex modes may be excited within the resulting cavity; exact analysis of these fields is a difficult problem, and the viability of supression techniques is unclear. Maximum values of RCS may be estimated by procedures outlined above. These values show that the ratio of controlled (reflector) to uncontrolled (missile) radar cross section is given by the ratio of the squares of the areas involved, i.e., for a 10 in. diameter nozzle,

$$\frac{(11)(11)}{(\pi x 5^2)^2} = -17.07\ dB,$$

illustrating the need for reduction of radar cross section of unaugmented portions of the missile for the case when a passive retroreflector is to be utilized.

D. RETROREFLECTOR LOSS FACTORS

The theoretical limit derived above can, in practice, never be achieved. Additional loss factors include (estimated losses):

TABLE 5. MAXIMUM RETROREFLECTOR RADAR CROSS SECTION

f (GHz)	λ (meters)	σ (m^2)	σ (dBm^2)
1	0.3	0.00659	-21.80
3	0.1	0.0593	-12.26
5.5	0.0545	0.20	-7.02
7	0.043	0.323	-4.90
9.5	0.03158	0.059	-2.28
16.5	0.01818	1.79	2.52
35	0.00857	8.075	9.07
70	0.00429	32.30	15.09
95	0.00316	59.49	17.74

- Polarization mismatch (circular from ground to linear on missile) 3 dB
- Collector coupling and mismatch losses 2 dB
- Aperture inefficiency 2 dB
- Retroreflector directivity—due to misalignment of retroreflector axis and loss to radar

The last of these factors is a function of the backscattering characteristics of the retroreflector, the missile trajectory, and the range to the missile. In order to analyze the magnitude of some of these effects, a parabolic trajectory with a QE of 40° and 40 km range was analyzed. A Van Atta-type array was assumed for the retroreflector because of its large backscattering angle and its simplicity of implementation. A variation in radar cross section of $[\sin(\pi/2\cos\phi)]^4$ was assumed [27]. Results are summarized in *Table 6*, indicating that the Van Atta array can hold directivity losses to rather small levels.

4. FREQUENCY TRADEOFF ANALYSIS

A central tradeoff in overall system design involves the choice of operating frequency. This is a somewhat complex analysis, involving a number of factors, including available transmitter devices; backscattering from the missile; attenuation and backscattering of the propagation medium; characteristics of the antenna, waveguide and component losses; and noise figure, to mention only a few.

To simplify the frequency tradeoff, two basic analyses were performed. The first analysis assumed a constant-size aperture (until the beamwidth became unreasonably small), while the second utilized a constant-beamwidth configuration. Comparisons were made of the single pulse received power as a function of range to the missile for the cases of both a passive reflector located on the missile and of an active beacon on board. However, in most cases, the constant-aperture condition was the one which most realistically reflected the system constraints of physical size and is the only one presented here. A detailed analysis of effects of signal-processing techniques was not carried out since it was felt that improvements resulting from such processing would be equally applicable to all such systems. It should be noted that the choice of different aperture sizes would change the numerical results of the analysis but not the relative levels of performance as a function of frequency.

Results of these analyses indicate that in clear air, one would maximize signal-to-noise ratio (SNR) by going down in frequency for the constant-beamwidth case, while one would maximize SNR by going up in frequency for the constant-aperture case. When one considers effects of atmospheric attenuation for rain rate of 4

TABLE 6. LOSS FACTOR DUE TO RETROREFLECTOR DIRECTIVITY — 40 km RANGE, 40° Q.E. — VAN ATTA ARRAY

Range (km)	Missile Altitude (km)	Missile Altitude (deg)	Reflector Angle, θ (deg)	Reduction in RCS, dB
1	0.81	38.59	0.42	0.00
3	2.32	35.53	2.37	0.00
5	3.67	32.21	4.07	0.00
10	6.29	22.78	9.39	0.00
15	7.87	11.86	15.82	0.03
20	8.39	0	22.76	0.13
25	7.87	-11.86	29.33	0.35
30	6.29	-22.78	34.59	0.68
35	3.67	-32.21	38.20	1.00
40	0	-40.00	40.00	1.20

mm/hr, one finds that SNR is maximized for X-band (9.5 GHz) operating frequencies for the constant-aperture comparison. An exhaustive analysis of the constant-beamwidth case was not further considered, since it was felt that the antenna aperture size limit represented a more realistic comparison.

Details of the analysis are presented in the following section.

A. CONSTANT APERTURE COMPARISON FOR A PASSIVE REFLECTOR

The case for the missile tracking radar system operating with a 5-ft aperture tracking a target consisting of a passive missile reflector was initially analyzed. Representative system parameters are presented in *Table 7*. Frequencies were selected as being in the major radar bands over the frequency range of interest. Antenna gain and bandwidth were for a 5-ft (1.52 m) aperture reflector antenna using

$$\theta \text{ (beamwidth)} = 70\lambda/d$$

where

θ = beamwidth in degrees
λ = operating wavelength
d = antenna diameter.

and

$$G = 10 \log_{10} (30{,}000/\theta^2)$$

where G = the gain in dB, relative to isotropic. However, once beamwidth became less than 0.4 deg, a constant beamwidth was used because of pointing and acquisition problems associated with narrow beamwidths. Peak transmitted powers were selected as being representative of easily fieldable technology at each frequency, as were the noise figures. Losses were those associated with a 5-ft length of standard waveguide, and reflector cross section was obtained from Section 3. Pulse rate frequency was selected to give an unambiguous range of approximately 40 km and pulse width was chosen to yield a transmitter duty cycle of 0.001, a value representative of many magnetron-type transmitter tubes. The receiver bandwidth was chosen as the reciprocal of the transmitted pulse width.

These radar parameters were then inserted into the free space radar equation to yield a value of received power as a function of range:

$$P_r = \frac{P_t G^2 \lambda^2 \sigma}{(4\pi)^3 R^4}$$

where

P_r = received power
R = range to the missile.

This value was then converted to dBm, losses accounted for, and compared with the equivalent noise power for a 4 mHz bandwidth and the specified noise figure to

TABLE 7. RADAR PARAMETERS CONSTANT APERTURE COMPARISON

	5.5 GHz	9.5 GHz	16.5 GHz	35 GHz	70 GHz	95 GHz
Wavelength (m)	.0545	.0316	.018	.0086	.0043	.0032
Antenna Gain (dB)	36.8	41.5	46.3	52.7	52.7	52.7
Peak Power (kW)	1000	250	125	100	10	5
Pulse Width (ns)	250	250	250	250	250	250
PRF (pps)	3750	3750	3750	3750	3750	3750
Rcvr Bandwidth (MHz)	4	4	4	4	4	4
Noise Figure (dB)	7	9	10	11	12	12
Losses (dB)	0.1	0.2	0.9	1.0	5.0	7.5
Reflector RCS (dBm)	-7.02	-2.28	2.52	9.07	15.09	17.74
Antenna Beamwidth (deg)	2.5	1.45	0.84	0.4	0.4	0.4

determine the SNR. SNR as a function of range is plotted in *Figure 10* for the system whose parameters are given in *Table 7*.

Examination of *Figure 10* shows that the single pulse SNR is maximized at 35 GHz; however, it should be emphasized that this is for the clear air condition. When rain at rates up to 4 mm/hr is taken into account, the picture changes somewhat.

Using data of Section 2, it is determined that for a 4 mm/hr rain rate, two-way attenuations of 0.12 dB/km are experienced at 9.5 GHz, 0.48 dB/km at 16.5 GHz, and 2.25 dB/km at 35.0 GHz; it is anticipated that it would be negligibly small at 5.5 GHz. Incorporating these data into this analysis, the behavior shown in *Figure 11* for SNR as a function of range is obtained.

Data presented in *Figure 11* show that maximum performance at 40 km range is achieved at an operating frequency of 5.5 GHz, but operation at 9.5 GHz gives similar performance. For ranges less than approximately 12 km, operation at 16.5 GHz provides enhanced SNR.

A final consideration when comparing the various frequencies is that of target-to-rain clutter ratios which would be encountered when operating in rain rates of up to 4 mm/hr. Data summarized in Section 2 indicate a radar cross section per unit volume, σ_v, of -68.6 dB m^2/m^3 at 9.4 GHz; -60.46 dB m^2/m^3 at 16 GHz; and -48.74 dB m^2/m^3 for operation at 35.0 GHz. Applying these values to the radar systems described in *Table 7*, one obtains variations in target-to-rain clutter ratio with range as given by *Figure 12*. Thus, the signal-to-rain clutter ratio is maximized at 35 GHz but is only slightly lower at 95 GHz and 16.5 GHz. Also note that signal-to-clutter ratios are such that coherent processing can provide significantly enhanced performance due to the large differential radial velocity existing between the missile and rain clutter.

B. CONSTANT APERTURE COMPARISON FOR A MISSILE WITH AN ACTIVE BEACON

In the analysis presented in the previous paragraphs, there are a number of problems which can be identified, even with this cursory analysis. Signal-to-clutter ratio is a significant problem for operation in the rain, probably necessitating that coherent Doppler processing be utilized. To improve signal-to-noise ratios, pulse-to-pulse integration may well need to be employed. In addition, depolarized scattering from the remainder of the missile may be a significant problem, as may ground clutter during the initial acquisistion phase. All of these problems may be alleviated by use of an active beacon on the missile which is offset in frequency from the ground-based interrogator.

Recent developments in solid-state sources hold considerable promise for

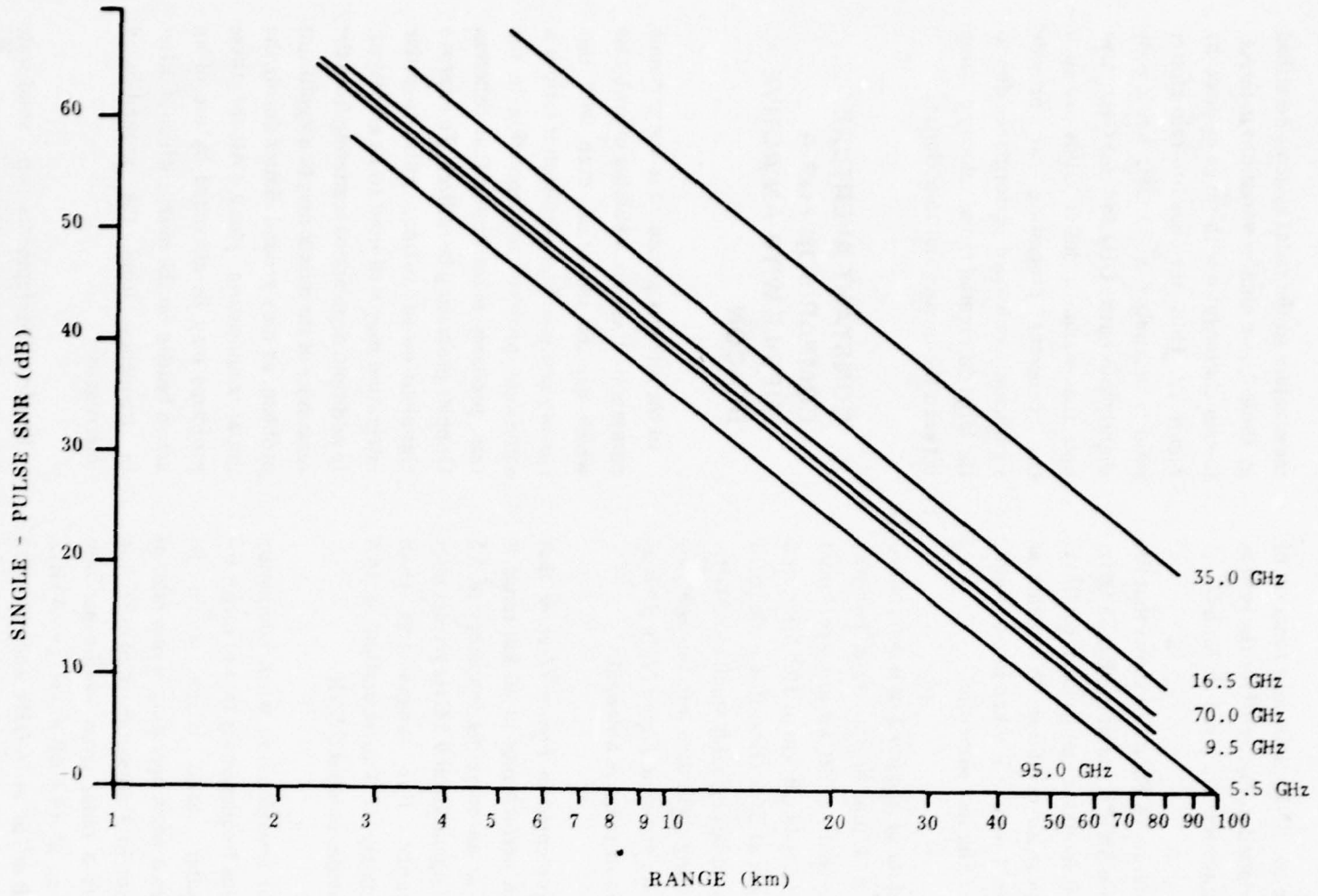

Figure 10. Single pulse SNR versus range for constant aperture systems defined in Table 1 for clean air conditions.

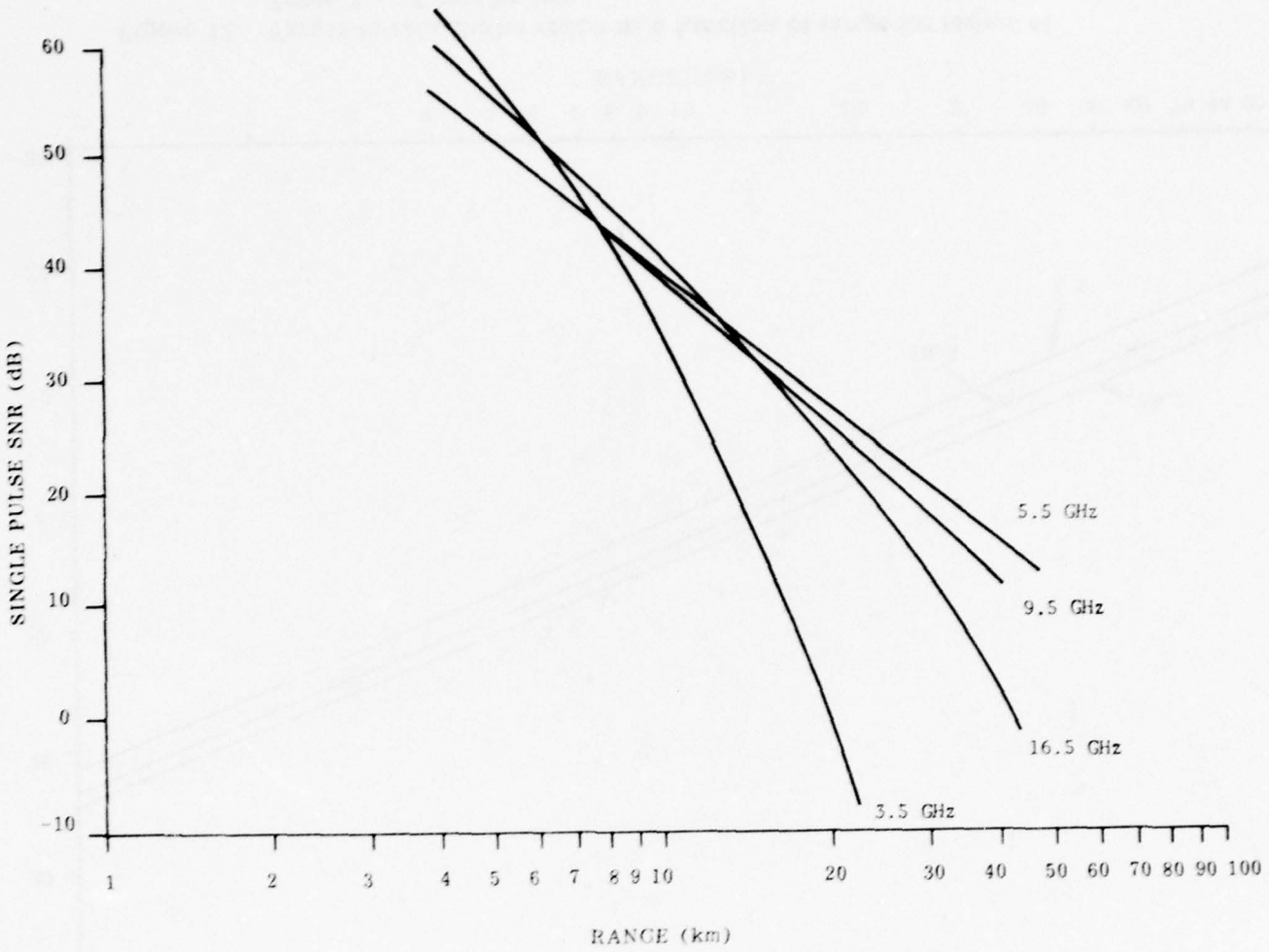

Figure 11. Single pulse SNR for radars of *Table 7 — 4 mm/hr rain.*

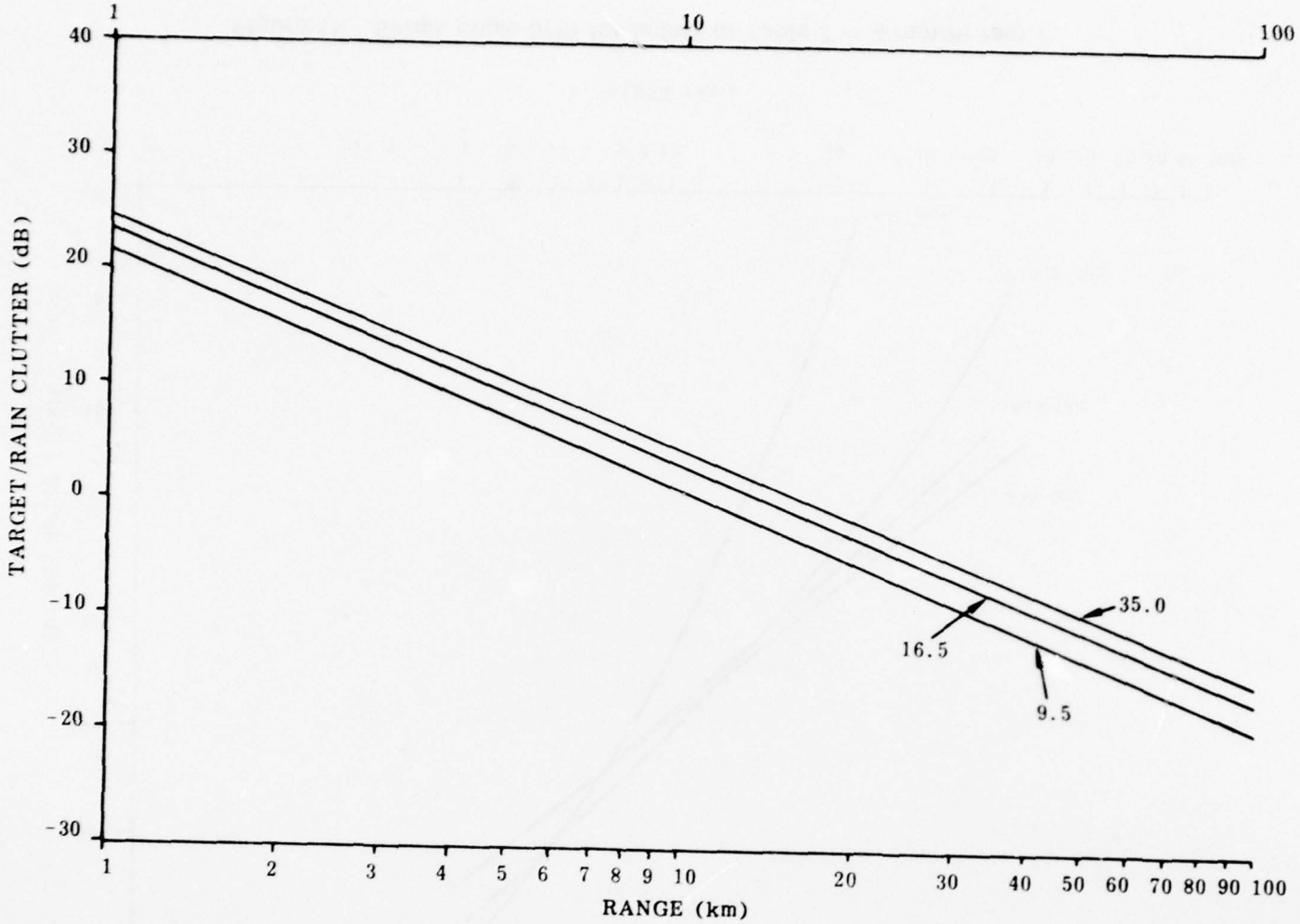

Figure 12. Target-to-rain clutter ration as a function of range for radars of Table 7 — 4 mm/hr rain.

reducing size, weight, power consumption and cost of beacon systems. A set of representative radar and missile parameters is given as *Table 8*. Missile antenna gain was calculated on the basis of the allowable area on the rear portion of one fin for an antenna, while the peak power was chosen to be compatible with available solid-state sources. Parameters summarized in *Table 8* were used in the beacon radar equation to calculate values of received power,

$$P_r = \frac{P_t G_T G_r \lambda^2}{16\pi^2 R^2} ,$$

and then losses, noise figure and receiver bandwidth were used to calculate signal-to-noise ratios as a function of range, which are summarized in *Figure 13*. These data show that SNR is maximized at 9.5 GHz, but that all of the frequencies analyzed offer adequate SNR for almost any application.

Operation during rain degrades performance of a beacon system also; however, effects are not as severe, because of the larger initial SNR and because only one-way attenuation (as opposed to two-way attenuation) must be accommodated. Again, referring to Section 2, one-way attenuation values of 0.06, 0.24, and 1.13 dB/km were calculated at 9.5, 16.5, and 35.0 GHz, respectively. Application of these values to *Figure 13* reduces SNR, but even for the 35 GHz case at 40 km where one-way attenuation is 45.2 dB, an SNR of approximately 20 dB is achieved.

Thus, the beacon case offers the advantages of improved SNR, essentially no rain or ground clutter, and freedom from polarization effects associated with missile backscattering, to name only a few, but requires increased cost per missile for additional on-board equipment.

5. SYSTEM ACCURACY ANALYSIS

The primary contributors to angular and/or range error estimates of target position for a tracking radar are:

- Radar-Dependent Tracking Errors
  - Thermal Noise
  - Multipath
  - Antenna Boresighting
  - Wind Loading
  - Servo Noise
- Target-Dependent Tracking Errors
  - Glint
  - Scintillation
  - Dynamic Lag
- Radar-Dependent Translation Errors
  - Pedestal Leveling
  - Azimuth Alignment
  - Pedestal Flexure
  - Data Take-Off Nonlinearity and Resolution

TABLE 8. RADAR PARAMETERS BEACON SYSTEM

Frequency (GHz)	5.5	9.5	16.5	3.5	70	9.5
Wavelength (m)	.0545	.0316	.0182	.0086	.0043	.0032
Beamwidth (deg)	2.5	1.45	.84	.4	.4	.4
Radar Antenna Gain (dB)	36.8	41.5	46.3	52.7	52.7	52.7
Missile Antenna Gain (dB)	14.49	19.24	24.03	30.56	36.57	39.23
Beacon Peak Power (w)	100	100	10	5	0.5	0.1
Pulse Length (ns)	250	250	250	250	250	250
PRF	3750	3750	3750	3750	3750	3750
Rcvr Bandwidth (MHz)	4	4	4	4	4	4
Noise Figure (dB)	7	9	10	11	12	12
Losses (dB)	0.1	0.2	0.9	1.0	5.0	7.5

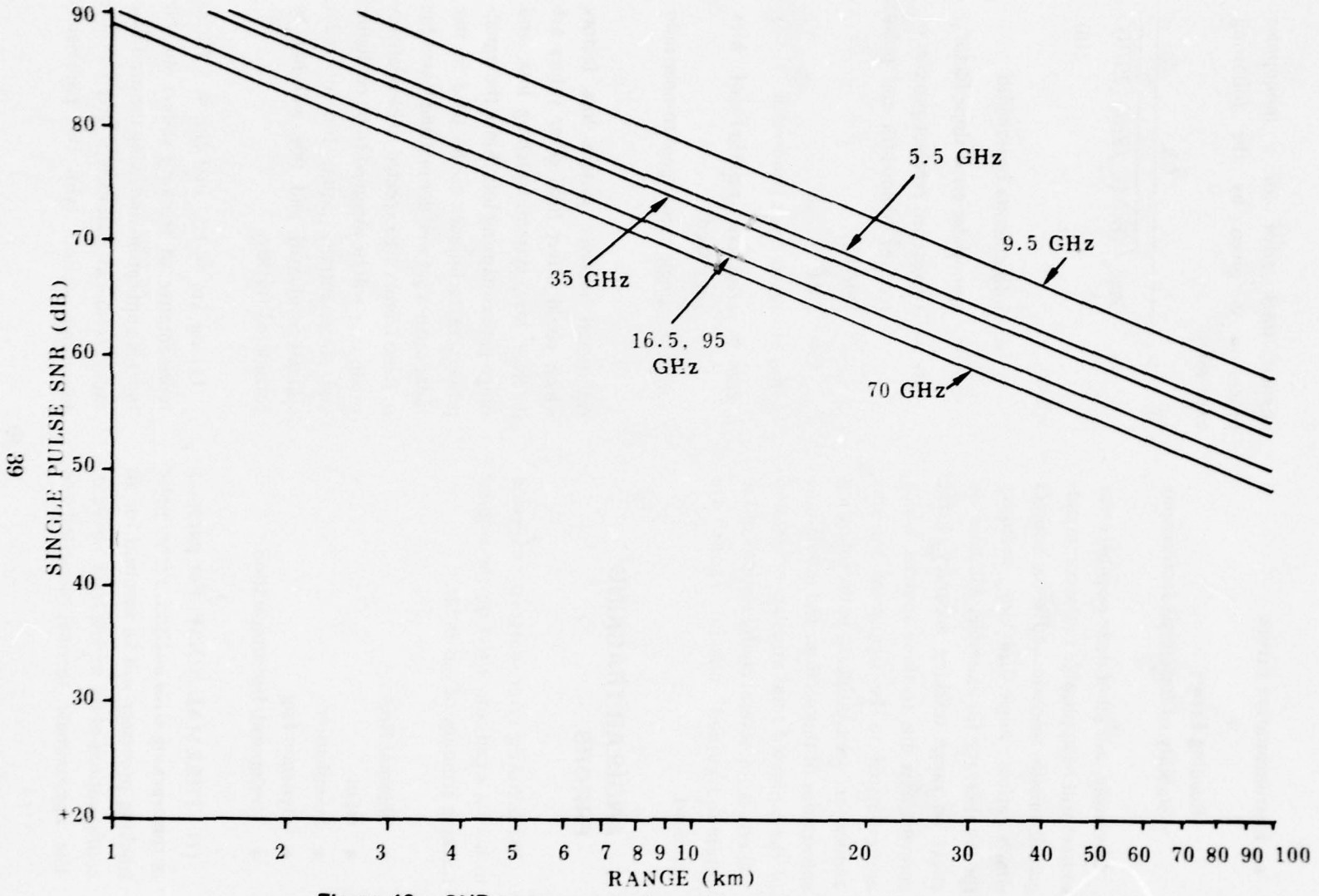

Figure 13. SNR versus range for radars of Table 8 — clear air.

- Instrumentation Errors
  - Reading Errors
  - Stability of Reference Instruments

Obviously, not all of these possible error sources will be applicable to the command-guided missile scenario and some sources which affect angle tracking accuracy (pedestal errors, for example) will have no effect on range tracking accuracy. Error contributions due to these sources, which are estimated to be significant for this application, are considered in the following subsections of this section, and tabulations of the estimated total angular, range, and roll errors for several configurations of the command-guided missile radar are presented.

A. ANGULAR TRACKING ERRORS

The following error sources are expected to have a significant effect on the angular tracking accuracy of this radar:

- Thermal Noise
- Glint
- Scintillation
- Dynamic Lag
- Mechanical/Instrumentation

(1) THERMAL NOISE. For purposes of this tracking error analysis, a monopulse tracking processor will be assumed for all configurations of the missile tracking radar. The approximate thermal noise-induced angular track error for a monopulse processor is given by the following expression:

$$\sigma_t = \frac{\theta_3}{km\sqrt{(B\tau)(f_r/2\beta m)(2S/N)}} \quad (10)$$

where

θ_3 = 3 db antenna beamwidth

km = monopulse error slope factor

$B\tau$ = 1 (matched receiver product of receiver bandwidth and pulse length)

f_r = PRF

βm = servo noise bandwidth

$f_r/2\beta m$ = effective number of hits smoothed

S/N = single pulse signal-to-noise ratio

Additional receiver system loss factors which could affect final error values are detector loss, system matching loss, and range-gate collapsing loss. Since the signal-processing techniques to be used in this radar are not yet well defined and losses due to these factors are expected to be relatively small, they will be assumed to be negligible and/or essentially equal for all radar systems evaluated and this will not be considered further.

Taking km = 1.57 and βm = 5 Hz as representative of tracking radars suitable for this application and using the candidate radar technical parameters given in the preceding section, with the parameters

pertinent to the track error analysis reproduced below, Equation (10) can be solved for the thermal noise angular tracking error, σ_t, as a function of single-pulse signal-to-noise ratio.

$$\sigma_t = \frac{\theta_3/43}{\sqrt{S/N}} \qquad (11)$$

for the following radar configurations.

Frequency (GHz)	θ_3 (degree)	f_r (Hz)	β_m (Hz)	km
9.5	1.45	3750	5	1.57
16.5	0.84	3750	5	1.57
35.0	0.4	3750	5	1.57

The thermal noise-induced angular error is plotted in *Figure 14* as a function of received S/N for the three sets of radar parameters given above. If the receive S/N $\geq$ 10 dB, the angular error is less than 0.18 milliradian for all three radars. The angular error at any range can be determined from this set of curves by obtaining the S/N ratio at the range of interest from curves given in the preceding section and then reading the angular error from *Figure 14* at this S/N.

(2) GLINT AND SCINTILLATION. Scintillation error for the monopulse tracker is zero since each estimate of target position is made on a single pulse rather than on a sequence of pulses. For a target with a uniform distribution of scatterers over a linear dimension, the angular glint error, σ, is given in radians by

$$\sigma = 0.35 \cdot L_x/R \qquad (12)$$

where L_x is the effective cross-range target dimension or span (cross-range distance between major scatterers), and R is the range to the target. In lieu of definitive data on glint from the missiles of interest, this equation is generally accepted as representing an upper bound on the expected glint-induced error. For purposes of this analysis, two cross-range spans were used: an L_x of 22 inches which corresponds to two primary scatterers located at the tips

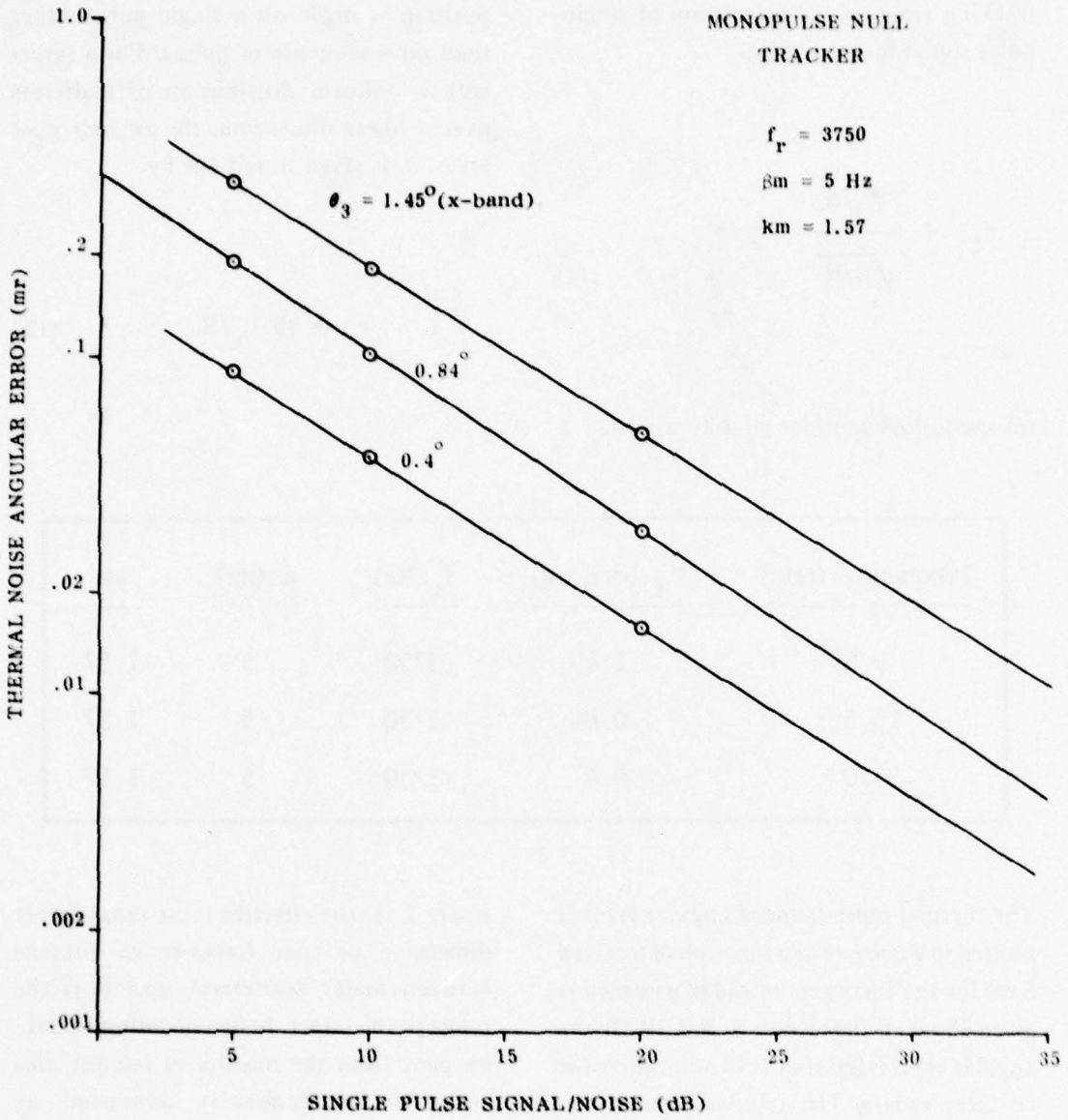

Figure 14. Thermal noise tracking error.

of two 5 1/2 inch horizontal stabilizing fins on an 11 inch diameter missile, and an L_s of 5 1/2 inches which corresponds to assuming two primary scattering centers separated by the length of one stabilizing fin. The calculated glint-induced errors for these two assumptions are given in *Figure 15* as a function of target range. These values should be considered as conservative estimates and as upper bounds on the glint-induced tracking errors for this radar.

(3) DYNAMIC LAG. The servo or tracking filter dynamic lag error in tracking a target is determined by the values of the servo/track filter error constants and by the real and apparent velocity, acceleration, and higher derivatives of target angle viewed by the radar. If the target has a linear velocity V_m and acceleration A_m, the radar will see angular components given by

$$W_m = V_m/R \sin A \qquad (13)$$

and

$$\dot{W}_m = A_m/R \sin B \qquad (14)$$

where W_m is the real angular rate of the target, R is the target range, and A and B are the angles between the V_m and A_m vectors, respectively, and the radar beam. In addition to these rates and higher derivatives due to A_m, which are limited by the maneuverability of the target, there are apparent or "geometrical" accelerations and higher derivatives which are caused by the radar observing the target in a spherical coordinate system. Thus, even a target moving at a constant rate in a straight line will cause the angle servos and tracking filters to operate with varying rates, depending upon the location of the target with respect to the radar and the direction of the velocity vector.

Figure 16 illustrates the geometry of the radar tracker/missile launcher combinations and a typical missile trajectory. The missile launcher and radar tracker are assumed to be co-located. Other than the relatively small azimuthal motion to correct the trajectory path and reduce impact error and, perhaps, trajectory deflections due to wind and missile spin and asymmetrical shape forces, almost all angular motion associated with this geometric scenario is confined to the elevation plane, with the maximum rates occurring after apogee on the downleg of the trajectory. Following relationships developed by Barton [28] for the *peak* or maximum values of the angular tracking rates in the elevation plane,

$$\dot{E} = W_e = V_m/R \qquad (15)$$

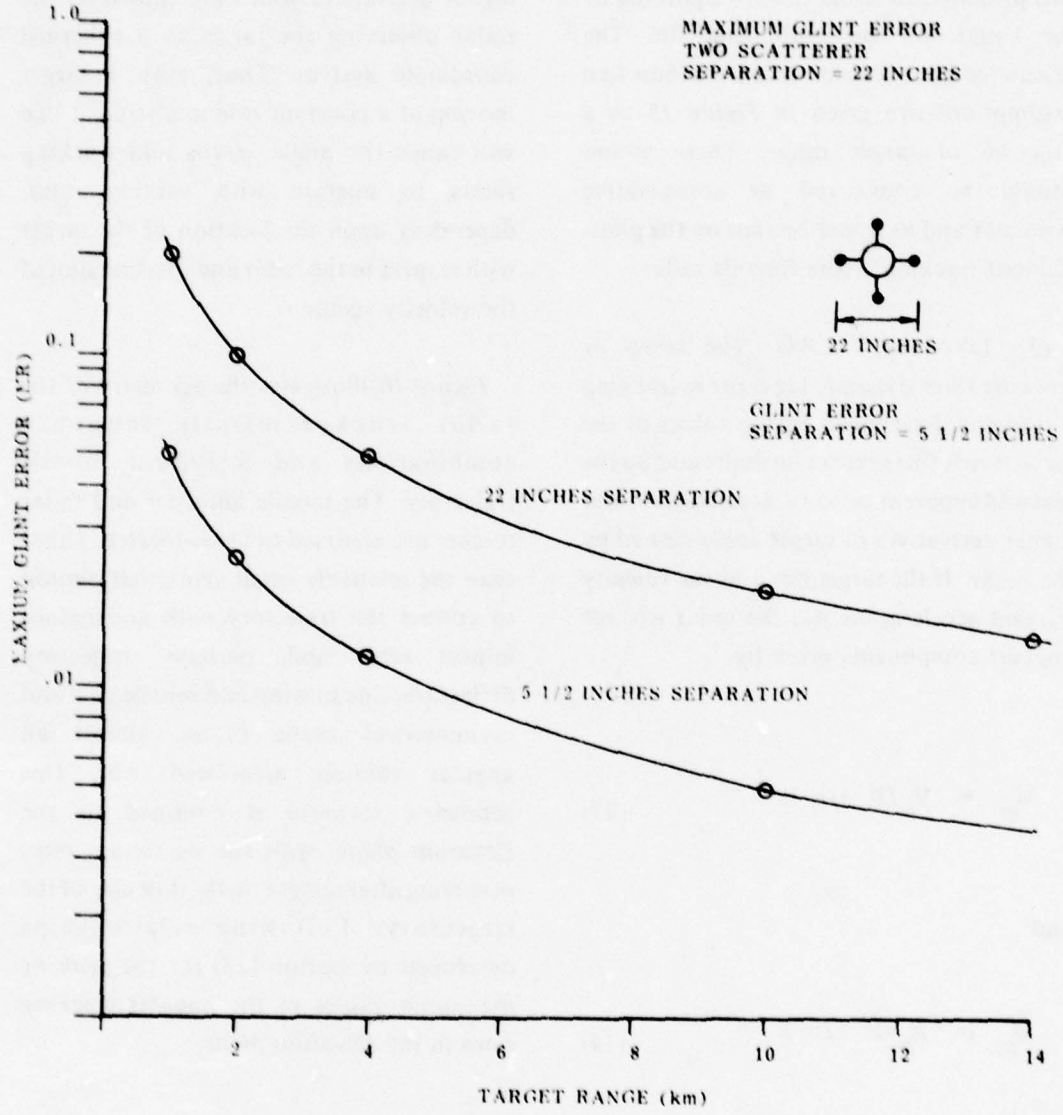

Figure 15. Glint tracking error.

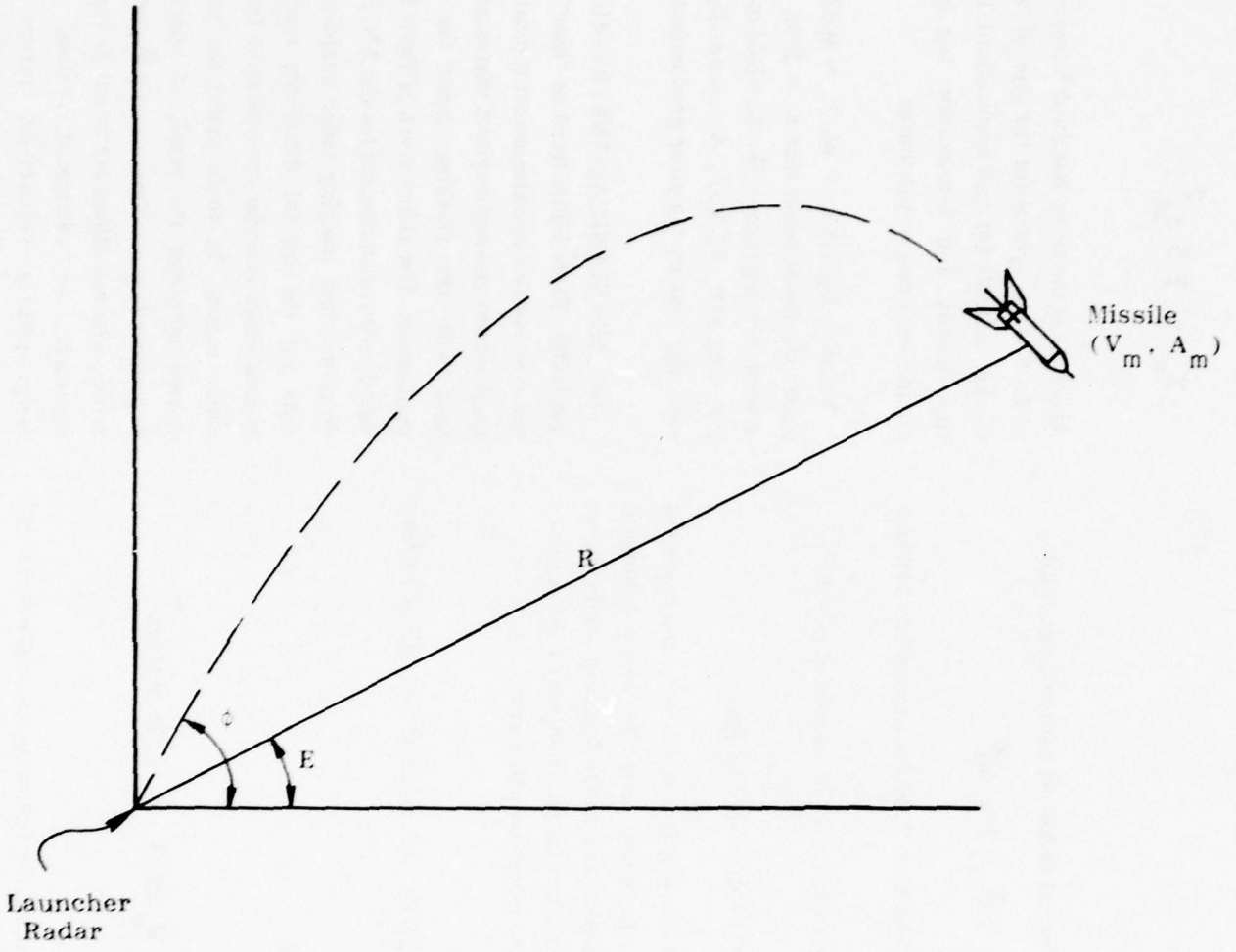

Figure 16. Geometry of radar tracker/launcher combination.

$$\ddot{E} = \dot{W}_e = 0.65(V_m/R)^2 + A_m/R \qquad (16)$$

under the following assumed conditions:

$$12^\circ \leq \phi \leq 40^\circ$$

$V_m(MAX)$ = 2200 fps (maximum downleg trajectory for 11 in. missile at $\phi = 12^\circ$)

$A_m(MAX)$ = -g (32.2 fps)

and selecting R = 30 km as representative of the maximum range at which command guidance and radar tracking might cease, the maximum radar angular tracking rates in the elevation plane are:

$$W_e(MAX) = 671/30 = 22.4 \text{ mr/sec}$$

and

$$\dot{W}_e(MAX) = 0.66 \text{ mr/sec}^2.$$

Making the following assumptions for the velocity, K_v, servo or track filter "error constant" and recalling that the acceleration error constant, K_a, is related to the servo bandwidth for a first- or second-order system by the following relationship,

$$K_a = 2.5\,\beta_m^2 \qquad (17)$$

where β_m is the servo bandwidth (assumed to be 5 Hz as typical for the type of radar tracker suitable for this application), both the velocity and acceleration lag error components can be calculated.

Velocity lag error = W_e/K_v = 0.02 mr under the assumption that K_v = 1000, and acceleration lag error = W_e/K_a = 0.01 mr for a $K_a = 62.5$ [$K_a = 2.5(5)^2$]. As is normally the case, the velocity lag error predominates.

(4) MECHANICAL/INSTRUMENTATION. *Table 9* lists fixed or "bias" and noise or variable tracking errors typical of a track mount and servo system that might be used with the tracking radar for this application. The values given in *Table 9* are based on errors measured for the AN/FPS-16 monopulse tracking radar modified by data for the optical theodolite tracking mount which is under consideration for the radar mount. In some cases, the values shown represent the result of operating experience (e.g., collimation and alignment error), whereas others are based on typical measured, or calculated, values. The tropospheric refraction terms are representative of typical conditions where the target is about 5° above the horizon. The total (noise and bias) tracking error

TABLE 9. MECHANICAL/INSTRUMENTATION ERRORS

Error Source	Angle Error in Mils rms	
	Bias	Noise
Boresight Axis Collimation	0.025	-
Boresight Axis Drift	0.04	-
Wind Loading (50 mph)	0.02	0.012
Servo Noise & Unbalance	0.01	0.02
Radar Dependent Tracking	0.052	0.023
Leveling, North Alignment	0.015	-
Orthogonality of Axes	0.02*	-
Mechanical Deflections	0.01	-
Thermal Distortion	0.01	-
Bearing Wobble	-	0.02*
Data Gear Error	-	0.03
Encoder Error	-	0.025(16 bits)
Radar Dependent Translation	0.029	0.044
Tropospheric Refraction	0.05	0.03
Total rms Error	0.078	0.058

*From Tracking Mount Design Requirements

resulting from the mechanical instrumentation factors given in *Table 9* is

$$\sqrt{(0.078)^2 + (0.058)^2} = 0.1 \text{ mr.}$$

(5) TOTAL ANGULAR TRACKING ERROR. Referring to curves in Section 4, which give S/N versus range for both clear and 4 mm/hr rain propagation conditions, the single pulse received S/N ratio for the three radar systems (X-band, K_u-band, and K_a-band) under consideration can be determined and then used in conjunction with *Figure 14* to estimate the thermal noise-induced angular tracking error. The calculated thermal noise error and received S/N ratio for both clear and 4 mm/hr propagation conditions are shown in *Table 10* for a radar-to-missile range of 30 km and additional system losses of 8 dB for the X-band radar, 11 dB for K_u, and 12 dB for K_a. These additional system losses are for a passive reflector RCS augmentation system on board the missile and generally result from such things as polarization mismatch at the missile, collector re-radiation coupling mismatch losses, augmentation antenna aperture inefficiency, and directivity losses due to the misalignment of missile axis and line-of-sight to the radar (antenna pattern losses).

The other angular tracking errors previously calculated in this section are also summarized in *Table 10* and the total rms angular tracking errors for each system are calculated and shown. For the assumed conditions, the X-band system gives the best overall tracking performance. The K_u- and K_a-band systems provide excellent tracking performance in the clear but degrade significantly in 4 mm/hr rain. In fact, these calculations indicate that the K_a-band system will not track in 4 mm/hr rain at a 30 km range.

B. RANGE ERROR ANALYSIS

The achievement of the desired range accuracy is one which involves a number of factors, including data quantization, transmitter jitter, lag, multipath, thermal noise, and the amount of pulse-to-pulse integration. Of these contributors, two – thermal noise and allowable amount of pulse-to-pulse integration – are limiting factors on system performance for this application. The rms range error due to thermal noise is given by [29]

$$\sigma_r = \frac{c\tau}{2\sqrt{2n\ S/N}} \qquad (18)$$

where

σ_r = the standard deviation of the range error,

c = the velocity of light,

τ = the effective pulse width (i.e., 1/B),

n = the effective number of pulses integrated,

and

S/N = the signal-to-noise power ratio.

TABLE 10. ANGULAR TRACK ERROR (MILS)

	X-Band		K_u-Band		K_a-Band	
	Clear	4 mm/hr	Clear	4 mm/hr	Clear	4 mm/hr
Thermal Noise (S/N-dB)	0.12 (13.5)	0.19 (10.0)	0.05 (15.5)	0.35 (0)	0.009 (25)	No Track
Glint	0.003	0.003	0.003	0.003	0.003	
Mechanical/Inst	0.10	0.10	0.10	0.10	0.10	
Velocity Lag	0.02	0.02	0.02	0.02	0.02	
Acceleration Lag	0.01	0.01	0.01	0.01	0.01	
TOTALS	0.16	0.22	0.11	0.364	0.10	No Track

Assume: R = 30 km

Systems Losses X-Band = 8 dB

K_u-Band = 11 dB

K_a-Band = 12 dB

However, when n is greater than one, the target will move between received pulses, possibly introducing additional uncertainty. In general, such total motion during the integration period should be kept small; however, for the highly deterministic flight paths of these missiles, one could shift time references from pulse to pulse in order to collect data from the target. To reduce system data-processing requirements, one would like to avoid this complexity; unfortunately, in many cases this is not possible.

To illustrate this fact, consider the requirement that target motion during the integration period be some small fraction, k, of the integrated range error. Then one can write:

$$\left(\frac{V_r}{prf}\, n\right) = \left(\frac{c\tau}{2\sqrt{2n\ S/N}}\right)\ k\ ;$$

solving for n, one obtains

$$n = \left(\frac{c\tau\ prf\ k}{V_r\ 2\sqrt{2}}\right)^{2/3} (S/N)^{-1/3}. \qquad (19)$$

Substituting

$$k = 1/3$$

$$V_r = 4788 \text{ fps}$$

$$c\tau = 125 \text{ ft}$$

and

$$prf = 3750,$$

one obtains

$$n = 5.11\ (S/N)^{-1/3};$$

for example, for an S/N ratio of 10, n = 2.37.

Such undesirably small values of pulses integrated make velocity correction quite desirable. The analysis for allowable numbers of pulses integrated is the same as the above case, but with ΔV_t replacing V_t, where ΔV_t is the uncertainty in velocity due to all causes.

Thus,

$$n = \left(\frac{c\tau\ prf\ k}{\Delta V_r\ 2\sqrt{2}}\right)^{2/3} (S/N)^{-1/3}. \qquad (20)$$

Substituting Equation (20) into Equation (18), one obtains

$$\sigma_r = \frac{c\tau}{2\sqrt{2(S/N)\left(\frac{c\tau\ prf\ k}{\Delta V_r\ 2\sqrt{2}}\right)^{2/3}(S/N)^{-1/3}}}$$

$$\sigma_r = \frac{(c\tau)^{2/3}}{2\sqrt{2}\left(\frac{prf\ k}{\Delta V_r\ 2\sqrt{2}}\right)^{2/3}(S/N)^{-1/3}} \quad (21)$$

If one assumes $\Delta V_r = 0.1\ V_r$, substituting into Equation (21), one obtains

$$\sigma_r = \frac{(125)^{2/3}}{2\sqrt{2}\left(\frac{prf\ k}{\Delta V_r\ 2\sqrt{2}}\right)^{2/3}}(S/N)^{-1/3}$$

$$= \frac{25}{2.68}(S/N)^{-1/3}$$

$$= 9.31\ (S/N)^{-1/3}$$

Table 11 tabulates a number of range errors and values of pulses integrated for a range of signal-to-noise ratios and the same data are presented in graphical form in *Figure 17*.

C. MISSILE ROLL ANGLE ERRORS

In order to correct the missile's trajectory accurately by firing small side thruster rockets on-board the missile, the instantaneous missile roll angle must be known. A polarization-based technique for providing this roll angle measurement information has been proposed and described herein. In essence, the signal retransmitted or reflected from the missile back to the radar will have a roll-referenced linear polarization. By measuring both receive polarization amplitudes simultaneously in a dual-channel polarimeter receiver, the polarization angle of the missile roll-referenced and linearly polarized signal can be measured by the radar and the absolute roll position of the missile determined continuously along the trajectory path.

However, both the depolarization efforts considered previously and receiver noise will corrupt this measurement and introduce errors. For the purposes of this analysis, assume that the missile RCS augmentation system either reflects or retransmits a linearly polarized signal which is referenced to the missile roll position. The objective of this analysis is to determine how accurately the radar receiver can measure the polarization angle of this rotating signal with respect to an absolute anglular reference in the presence of such previously considered depolarizing effects as the transmitting and receiving antennas,

TABLE 11. OPTIMUM NUMBERS OF PULSES INTEGRATED AND RESULTING ERRORS

Signal-to-Noise Ratio	Signal-to-Noise Ratio (dB)	Optimum Number of Pulses Integrated, m	Range Error, σ_r (ft)
1	0	24	9.08
5	7	14	5.31
10	10	11	4.21
20	13	9	3.43
50	17	7	2.46
100	20	5	2.01
200	23	4	1.55
500	27	3	1.14
1000	30	2	0.91

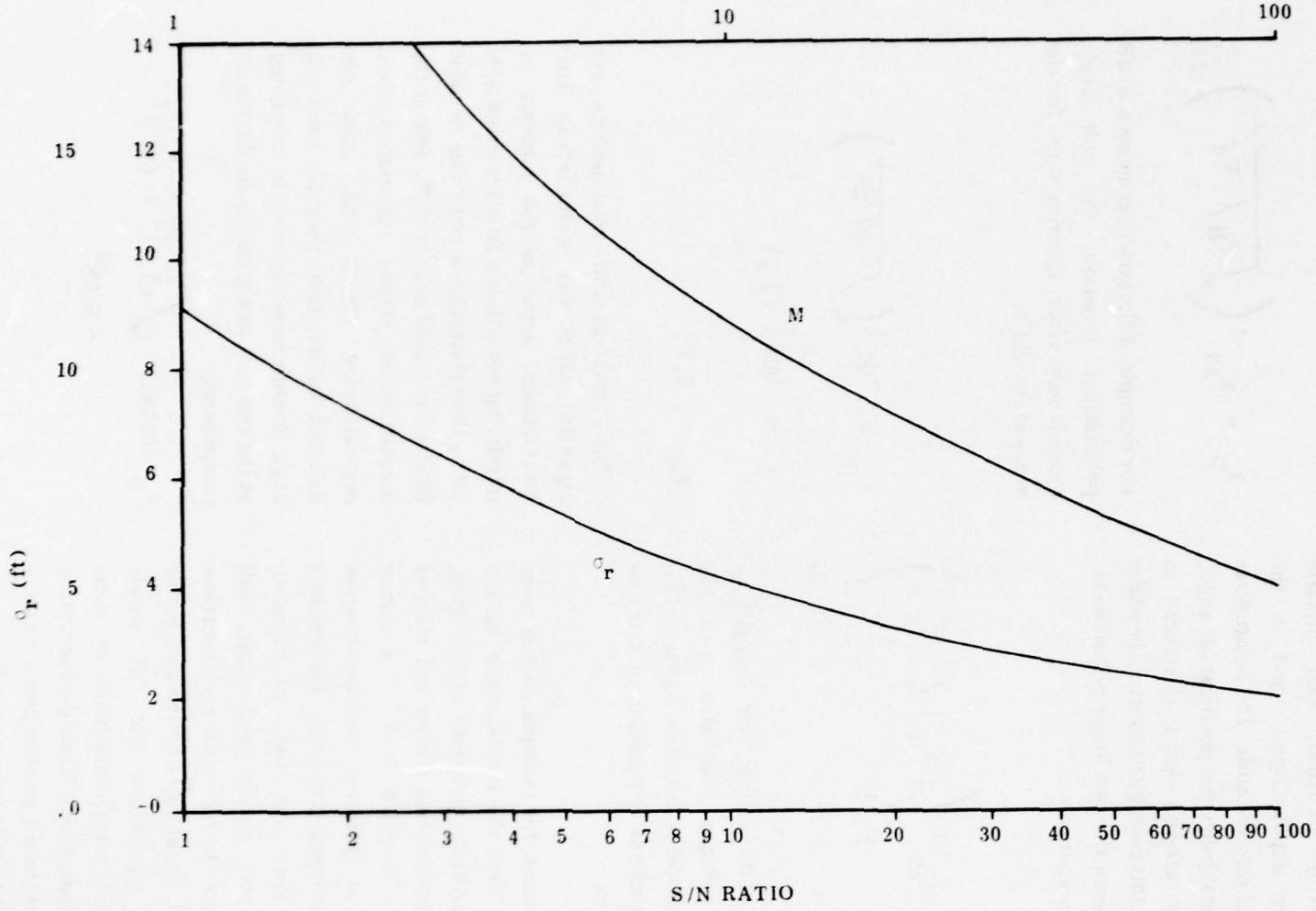

Figure 17. Optimum number of pulses integrated and thermal noise range error as a function of SNR. X = 1/3, = Vr = 479 fps, and c = 125 ft.

propagation medium, and missile backscatter depolarization, and in the presence of receiver noise. The polarimeter receiver establishes the polarization angle, θ_p, of the received signal, referenced to vertical in this case, by measuring the phase angle between the two linear polarization-received components

$$\theta_p = T_{AN}^{-1}\left(|\bar{E}_H| / |\bar{E}_V| \right) \quad (22)$$

where E_v is the electric field strength (or detected voltage) associated with the received vertical polarization signal and E_H is the horizontal component or received electric field.

If we assume, for example, that at some instant of time the missile sends back a "pure," vertically polarized signal, then, with no depolarizing effects and receiver noise, $E_H = 0$ and $\theta_p = 0^\circ$ – a perfect measurement. However, the depolarization effects considered previously, transmitting and receiving antennas, propagation medium, and missile backscatter, will generate a horizontal polarization component, E_H, at the radar receiver. In this case, θ_p represents the roll angle measurement error introduced by these depolarization effects. Since depolarization values are normally given as power ratios, a more convenient expression for θ_p is

$$\theta_p = T_{AN}^{-1}\left(\sqrt{P_H / P_V} \right) \quad (23)$$

For example, if the system achieves a 20 dB polarization isolation, the roll angle measurement error, ignoring noise for the moment, would be

$$\theta_p = T_{AN}^{-1}\left(\sqrt{-20\ \text{dB}} \right)$$

$$= T_{AN}^{-1}\ (0.1)$$

$$\theta_p = 5.7^\circ$$

The same general relationships are equally valid for calculating roll measurement error in the presence of interfering noise. For a 20 dB received S/N ratio, the measurement error due to noise limitations would also be 5.7°, and, if the measurement errors associated with depolarization effects and noise are assumed independent, then the total roll angle measurement error can be calculated as the rms sum of the two individual error components.

$$\theta_p\ (\text{total}) = \sqrt{(5.7)^2 + (5.7)^2}$$

$$= 8.08^\circ$$

Plotted in *Figure 18* are both the noise-only roll angle errors and the total error in estimating the absolute missile roll angle by measuring the roll-referenced received polarization for a system-induced depolarization ratio of -19 dB. Over a received S/N range of 7 dB to 20 dB, the roll angle measurement errors vary from a maximum of 25° at 7 dB to a minimum of 8.6° at 20 dB.

6. POSTULATED SYSTEM CHARACTERISTICS

The analyses to this point have indicated that it is feasible to design a radar/missile system for measurement of missile position and roll angle. Such a system has a number of unique characteristic/requirements, including:

- Radiation of circular polarization
- Reception of two orthogonal linear polarizations for roll angle measurement
- A monopulse tracking capability for azimuth and elevation determination
- Ability to operate in adverse weather
- Provision for precise missile range information

A number of key decisions need to be made in specifying such a system; the choice of transmitted frequency appears to lie somewhere around the 10 GHz region and was discussed extensively (including effects of adverse weather) in Section 4. Implementation of the GROWLAR concept using polarization for roll angle measurement at radar frequencies was discussed in Section 3, and the accuracies achievable with such a system are analyzed in considerable detail in Section 5.

The basic system parameters and types of signal processing which are required differ if an active beacon-transponder or a passive retroreflector are utilized on board the missile. The use of a passive retroreflector permits simplification of the missile but at the expense of a more complex and costly ground-based radar system. The use of a beacon on the missile (preferably offset in frequency from the radar transmitter) permits a substantial reduction in cost and complexity of the ground-based radar while requiring a more complex missile.

Simplifications associated with use of an active beacon/transponder on the missile include

- Elimination of pulse-to-pulse integration due to the large signal-to-noise ratios which would be realized
- Elimination of need for coherent (Doppler) processing if the transponder frequency is offset from the transmitted frequency

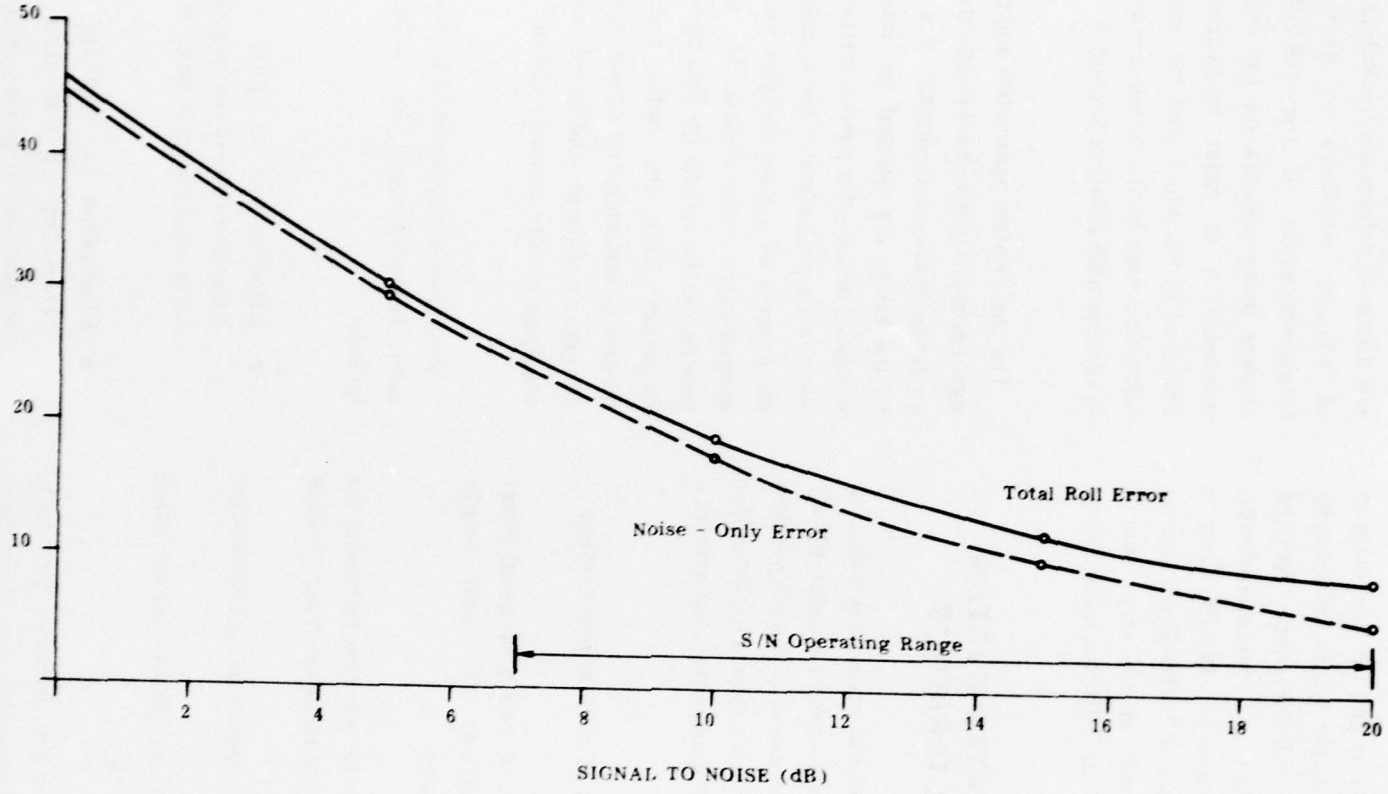

Figure 18. Missile roll angle errors; depolarization = -19 dB and depolarization error = 64°.

- Removing the effects of missile reflectivity from the signal received at the radar system

However, these substantial advantages must be weighed against the increased cost/missile associated with implementation of such a concept.

A compilation of characteristics of suitable candidate radar systems for a missile which uses a passive retroreflector and one which uses an active beacon/transponder are presented as *Table 12*, and a simplified block diagram of a system for use with a passive reflector is given as *Figure 19*. A block diagram of the system for the active beacon/transponder case would appear quite similar, but with the MOPA chain replaced with a magnetron transmitter and with the appropriate simplifications in the signal-processing portion of the system.

All portions of the systems described in *Table 12* and *Figure 19* are realizable using available technology. While the use of dual-polarized monopulse antenna for radiation of circular and reception of two orthogonal linear polarizations is somewhat unconventional, it is a relatively straightforward extension of earlier efforts on polarization agile and diverse antenna systems conducted at Georgia Tech [29,30]. Similarly, the choice of polarization for angle tracking based on the larger of the two linear received polarizations is somewhat unconventional but requires only conventional circuit techniques for implementation.

7. CONCLUSIONS AND RECOMMENDATIONS

Design calculations, performance tradeoffs and projections, and supporting technical data analysis, as they relate to the feasibility of a microwave or millimeter radar for providing position and roll data in a command-guided ballistic rocket concept, have been presented and discussed in the previous sections of this report. The primary conclusions evolving from these studies and analyses are summarized below:

1. A tracking system incorporating a passive reflector or active transponder-equipped rocket will satisfy total system requirements.

2. When compared with 5.5, 16.5, 35, 70, and 95 GHz radar systems, an X-band (9.5 GHz) radar tracker provides optimum performance.

3. Polarization techniques for determining missile roll angle with an accuracy of 5 to 15° are feasible at radar frequencies.

4. An active transponder on board the missile simplifies the tracking radar but results in more electronics on the missile and, consequently, a more expensive missile.

TABLE 12. MAJOR SYSTEM CHARACTERISTICS

Frequency	X-Band	X-Band
Peak Power	250 kW	250 kW
Pulse Length	0.25μsec	0.25μsec
Prf	3750 pps	3750 pps
Transmitter Type	MOPA Chain	Magnetron
Antenna	Dual Polarized Monopulse Paraboloid, 1.5° x 1.5° Beam-Transmit Circular, Receive Two Orthogonal Linear Polarizations	
Receiver	Coherent, Dual Polarized, Monopulse/ Polarimeter	Dual Polarized Monopulse/Polarimeter
Signal Processing	MTI/Doppler Filtering Pulse-to-Pulse Integration Angle Track/Smoothing Roll Angle Determination Tracking Polarization Selection	Angle Track/Smoothing Range Tracking/Smoothing Roll Angle Determinations Tracking Polarization Selection

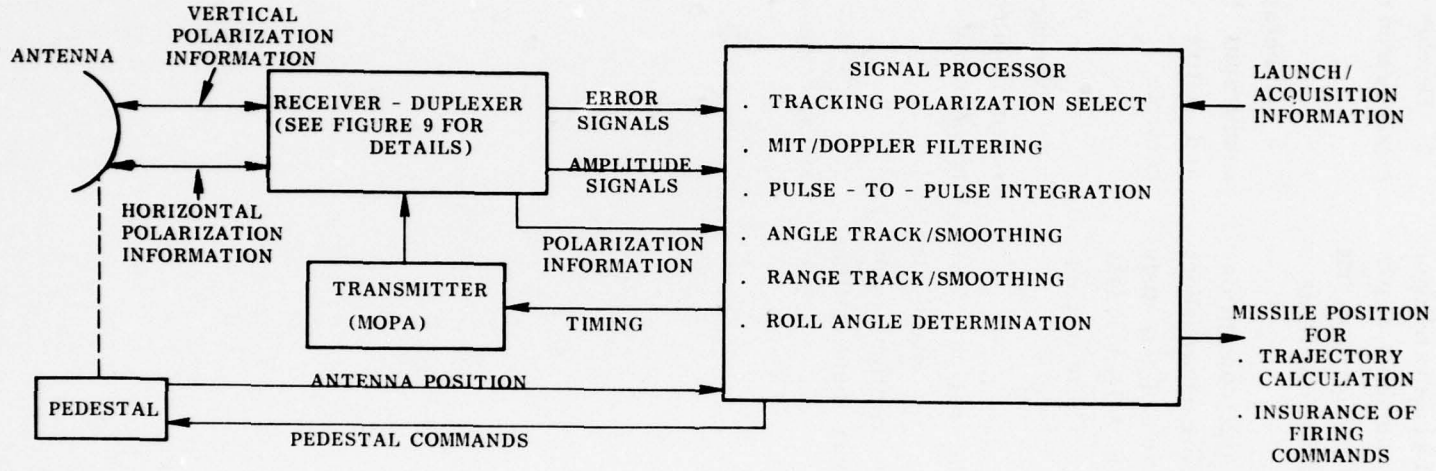

Figure 19. Simplified system block diagram for the ground-based radar for use with a missile employing a passive retroreflector.

5. Conversely, use of a passive reflector system on the missile simplifies missile electronics and reduces missile costs, but requires a more complex tracking radar.

Corresponding to the conclusions listed above, several recommendations were generated as a result of this study and discussions with MIRADCOM technical personnel. These recommendations are:

1. Initiate a theoretical and experimental program to investigate various retroreflector configurations and missile reflectivity polarization characteristics.

2. Develop a detailed design for a missile beacon transponder.

3. Generate cost tradeoffs and comparisons between passive reflector and active beacon-equipped rocket concepts.

4. Examine multiple rocket tracking system concepts and tracking radar requirements.

5. Develop "proof-of-concept" system design and demonstration plan.

REFERENCES

1. Fagan, J. J., et al., "Study of GROWLAR Add-On to GSRS," MIRADCOM Internal Memorandum Report.

2. Currie, et al., *Analysis of Radar Rain Return at Frequencies of 9.375, 36, 70, and 95 GHz*, Technical Report No. 2, Contract DAAA25-73-C-0256, February 1975.

3. Reedy, E. K., et al., *Performance and Cost Analysis of Battlefield Surveillance Moving Target Acquisition Radars*, Technical Report, Contract N00014-75-C-0320, May 1976.

4. Richard, V. W., and Kammeren, J. E., *Rain Backscatter Measurements and Theory at Millimeter Wavelengths*, BRL Report No. 1838, October 1975.

5. Oguchi, T. "Rain Depolarization Studies at Centimeter and Millimeter Wavelenghts: Theory and Measurement," *Journal of the Radio Research Laboratories*, Vol. 22, No. 109, 1975, pp. 165-211.

6. Evans, B. G., Fryatt, A. J., Read, J., and Thompson, P. T. "Investigation of the Effects of Precipitation on Parabolic Antennas Employing Linear Orthogonal Polarization at 11 GHz," *Electron Letter*, Vol. 7, July 1971, Vol. 7, pp. 375-377.

7. Crawford, A. B., Hogg, D. C., and Hunt, L. E. "A Horn-Reflector Antenna for Space Communication," *Bell System Technical Journal*, Vol. 40, July 1961, pp. 1095-1116.

8. Dragone, C., and Hogg, D. C., "The Radiation Pattern and Impetance of Offset and Symmetrical Near-Field Cassegrainian and Gregorian Antennas," *IEEE Trans. Antennas and Propagation*, Vol. AP-22, May 1974, pp. 472-475.

9. Hayes, R. D., et al., *Study of the Polarization Characteristics of Radar Targets*, Final Report on Contract DA-36-039SC-64713, October, 1958.

10. Clarricoats, P. J. B., and Saha, P. C., "Propagation and Radiation Behavior of Corrugated Feeds," *Proc. IEEE*, Vol. 118, No. 9, 1971, pp. 1167-1186.

11. Potter, P. D., "A New Horn Antenna with Suppressed Sidelobes and Equal Beamwidths," *Microwave Journal*, Vol. 6, No. 6, 1963, pp. 71-78.

12. Cohn, S. B., "Flare-Angle Changes in a Horn As a Means of Pattern Control," *Microwave Journal*, Vol. 13, No. 10, 1970, pp. 41-46.

13. Watson, P. A., and Ghobrial, S. I., "Off Axis Polarization Characteristics of Cassegrainian and Front Feed Paraboloidal Antennas," *IEEE Trans. on AP*, Vol. 20, No. 6, 1972, pp. 691-698.

14. Watson, P. A., and Ghobrial, S. I., "Cross Polarization in Cassegrainian and Front Fed Antennas," *Electron Letter*, Vol. 9, No. 14, 1973, pp. 297-298.

15. Wood, P. J., "Depolarization with Cassegrainian and Reflectors," *Electron Letter*, Vol. 9, Nos. 8/9, 1973, pp. 181-183.

16. Wood, P. J., "Cross-polarization with Cassegrainian and Front Fed Reflectors," *Electron Levver*, Vol. 9, No. 25, 1973, pp. 597-598.

17. Evans, B. G., and Thompson, "Use of Cancellation Techniques in the Measurement of Atmospheric Cross-polarization," *Electron Letter*, Vol. 9, No. 19, 1973, pp. 447-448.

18. Watson, P. A., et al., "Mutual Interference Between Linear Crosspolarized Radio Channels at 11 GHz," *Electron Letter*, Vol. 7, No. 13, 1971, pp. 374-375.

19. Evans, B. G., et al. "Investigation of the Effects of Precipitation on Parabolic Antennas Employing Linear Orthogonal Polarization at 11 GHz," *Electron Letter*, Vol. 7, No. 13, 1971, pp. 375-377.

20. Shimba, M., et al., "Radio Propagation Characteristics Due to Rain at 20 GHz Band," *IEEE Trans. on AP*, Vol. 22, No. 3, 1974, pp. 507-509.

21. Watson, P. A., and Ghobrial, S. I., Cross Polarizing Effects of a Water Film on a Parabolic Reflector at Microwave Frequencies," *IEEE Trans. on AP*, Vol. 20, No. 5, 1972, pp. 668-671.

22. Takano, T., et al., "Investigation of Snow Accretion and its Effect on 20 GHz Cassegrainian Antenna," Paper of Technical Group on AP, I.E.C.E. Japan, AP-74-26, 1974.

23. Evans, B. G., and Thompson, P. T. "Cross-Polarization Due to Precipitation at 11.6 GHz," *Journal de Recherches Atmospheriques*, Vol. 8, No. 1-2, 1974, pp. 129-136.

24. Oguchi, T., "Rain Depolarization Studies at Centimeter and Millimeter Wavelengths: Theory and Measurement," *Journal of the Radio Research Laboratories*, Vol. 22, No. 109, 1975, pp. 165-211.

25. Johnson, R. C., Cain, F. L., and Bone, E. N., "Dual-Mode Coupler," *IEEE Trans. on Microwave Theory and Techniques*, Vol. MIT-15, No. 11, November, 1967, pp. 651-652.

26. Van Atta, L. C., "Electromagnetic Reflector," U. S. Patent 2,908,002, October 6, 1959.

27. Sharp, E. D., and Diab, M. A., "Van Atta Reflector Array," *IRE Trans. on Antennas and Propagation*, Vol. AP-8, July 1960, pp. 436-438.

28. Barton, D., *Radar System Analysis*, Artech House, Inc., 1976.

29. Wallace, M. E., Ewell, G. W., and Stapleton, L. A., "Inertialess Polarization Scanners," Final Report on Contract DAAH01-67-C-1438, April 1968.

30. Rumsey, V. H., et al., "Techniques for Handling Eliptically Polarized Waves With Special Reference to Antennas," *Proceedings of the IRE*, May 1951, pp. 533-552.

APPENDIX A
MONOPULSE COMPARATORS

MONOPULSE ANTENNA FEED COUPLERS

MDL monopulse antenna feed couplers are designed from proven stock components, and provide excellent phase and amplitude control to assure deep nulls and minimum boresight shift with frequency. Dual polarization monopulses employing orthogonal transducers in conjunction with hybrid networks are available. This unique design permits the use of both horizontal and vertical polarization in any antenna feed system. Matching polarizers to generate circular polarization are also available upon request. Described here are just a few typical designs of the many monopulse antenna feed couplers available. MDL will be happy to quote on custom-designed monopulse antenna feed couplers to meet your special requirements.

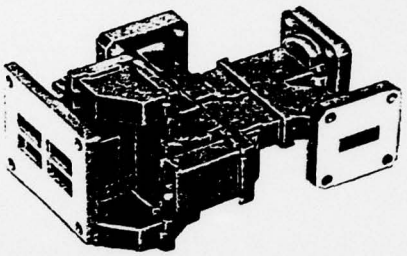

WG SIZE	OPERATING FREQ. (GC)	MODEL NUMBER	MAXIMUM VSWR SUM ARM	DIFF. ARM1*	DIFF. ARM2*	MIN. ISOLATION DB	MAX. OUTPUT POWER UNBALANCE ±DB	MAX. OUTPUT PHASE ERROR (SUM)	MAX. OUTPUT PHASE ERROR (DIFF.)	OUTPUT PHASE VARIATION VS. FREQ.
SINGLE POLARIZATION										
WR28	30.0 - 32.0	28CM26-1	1.30	1.50	1.40	30	.25	5°	4°	2.5°
	34.0 - 36.0	28CM16-1	1.30	1.50	1.40	30	.25	5°	4°	2.5°
WR42	23.0 - 24.0	42CM16-1	1.25	1.50	1.35	32	.15	5°	4°	2°
WR51	15.8 - 17.0	51CM16-1	1.15	1.25	1.25	40	.15	3°	2°	1°
WR62	15.5 - 17.0	62CM16-1	1.25	1.35	1.35	35	.15	3°	3°	2°
WR90	8.5 - 9.6	90CM26-1	1.15	1.25	1.25	40	.10	3°	2°	1°
	8.5 - 9.6	90CM46	1.15	1.25	1.25	40	.10	3°	2°	1°
WR112	7.1 - 8.5	112CM36	1.20	1.50	1.50	40	.10	3°	2°	1°
	7.35 - 8.3	112CM46	1.20	1.50	1.50	40	.10	3°	2°	1°
	7.5 - 8.5	112CM16	1.15	1.20	1.20	40	.10	3°	2°	1°
	7.5 - 8.5	112CM56	1.15	1.20	1.20	40	.10	3°	2°	1°
	7.55 - 8.4	112CM26	1.25	1.25	1.25	40	.10	3°	2°	1°
WR137	5.4 - 5.9	137CM26	1.15	1.20	1.20	35	.10	3.5°	1.5°	1°
	5.4 - 5.9	187CM16	1.15	1.20	1.20	35	.10	3.5°	1.5°	1°
WR187	5.4 - 5.9	187CM26	1.40	1.40	1.40	30	.10	6°	4°	2°
WR229	3.7 - 4.2	229CM16	1.20	1.30	1.30	40	.10	3°	2°	1°
WR284	2.7 - 3.15	284CM16	1.25	1.35	1.35	35	.10	3°	2°	1°
SINGLE POLARIZATION .150 HEIGHT										
WR90	8.5 - 9.6	C90CM16	1.20	1.25	1.25	40	.10	3°	2°	1°
DUAL POLARIZATION										
WR90	8.5 - 9.6	90CM66	1.30	1.25	1.25	40	.10	3°	2°	1°
WR187	5.4 - 5.9	187CM36	1.40	1.30	1.30	35	.15	3°	2°	2°

*Between any two adjacent arms that comprise a sum pattern.

**Between any two adjacent arms that comprise a difference pattern.

PRECEDING PAGE BLANK

APPENDIX B
THREE CHANNEL MONOPULSE IF SUBSYSTEM FOR DUAL AXIS PROCESSING

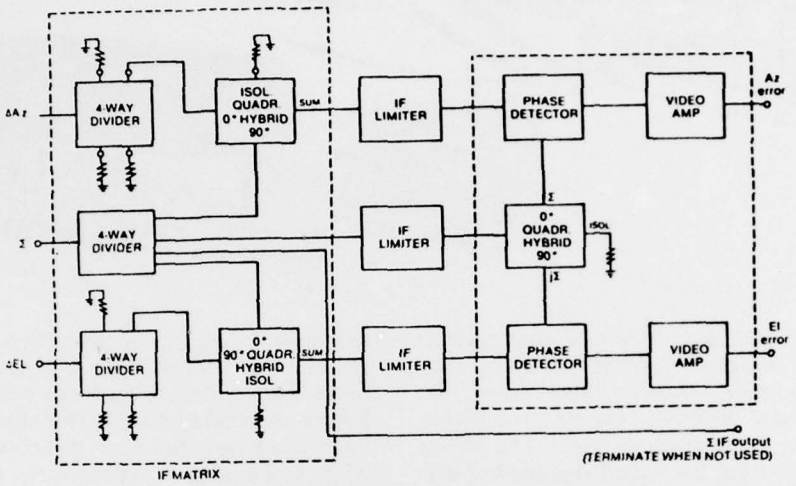

RHG now offers a complete 3 channel monopulse IF processing subsystem. The use of this subsystem removes the critical interface problems normally encountered by the system designer. The block diagram configuration is designed for in-phase signal inputs, and reflects a field proven, straightforward use of the necessary IF elements. Other input phase configurations can also be supplied when required.

While the subsystem is used mainly in return-to-boresight applications, it can also be used in angle-error types of systems.

Packaging is straightforward. An IF matrix, a detector matrix, and three matched limiter channels are all mounted to an aluminum baseplate, with all power connectors brought out to a single barrier strip. If desired, all the individual modules can be removed from the plate and be separately mounted in the user's system.

Model	Center Freq. (MHz)	Information BW (MHz)	Accuracy BW (MHz)	Settling Time (nsec)	Accuracy (degrees)	Price
MPD3010	30	10	2	0.1	±3	$4,750
MPD6010	60	10	2	0.1	±3	4,750
MPD6020	60	20	4	0.08	±3	4,900
MPD7020	70	20	4	0.08	±3	4,900
MPD16020	160	20	4	0.08	±5	5,500

ADDITIONAL SPECIFICATIONS

1. Accuracy is boresight error in electrical degrees (This is the ratio accuracy expressed in degrees)
2. Input dynamic range: +5 to −dBm
3. Input level difference: Δ channels can be up to 30 dB below Σ channel
4. Input Impedance: 50 Ω (VSWR 1.5:1 Mom)
5. Supplementary IF output: Approx. 7 dB below Σ channel input. Ideally suited for driving a log IF amplifier chan Impedance and dynamic range compatible with RHG ICLT log amps.
6. Video Output Impedance: 75 Ω (source VSWR ≤ 1.2:1).
7. Connectors: SMA
8. Power: ±12VDC (±15VDC available N/C, add Suffix "C")
9. Temperature vs. accuracy: 0 to 50 °C: rated accuracy −30 to +71 °C: ≤ twice rated degrees

NOTES:
1. See Glossary for detailed definition of terms 2. Special parameters, other frequencies, etc. are available—contact facto

RHG ELECTRONICS LABORATORY·INC
161 East Industry Court ■ Deer Park, New York 11729 ■ (516) 242-1100 ■ TWX 510-227-6083

PRECEDING PAGE BLANK

IF PHASE DETECTOR SUBSYSTEMS

■ Self-contained ■ Small size ■ IC construction ■ MIL grade
■ Tracking radars ■ Interferometers ■ Direction Finders ■ Test Equipment

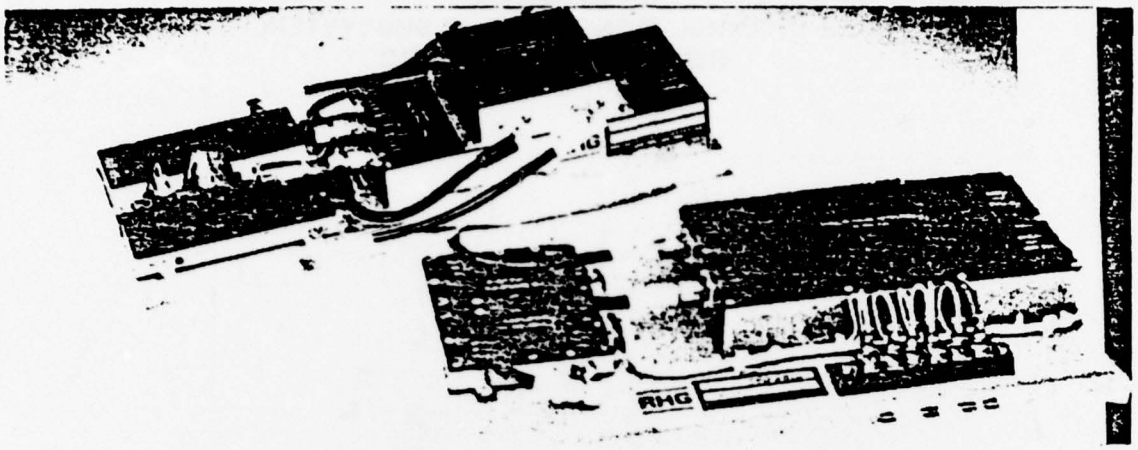

RHG now offers a line of complete IF phase detector subsystems. These phase detectors produce direct coupled video output(s) that are functions of the instantaneous phase difference between the IF inputs, over a wide range of input levels. The phase detectors are optimized for pulsed signals, but are equally useable for CW or analog inputs.

The phase detector subsystems are intended for use in monopulse and interferometer receivers as well as for use in instrumentation. They are complete subsystems, incorporating all necessary limiters, IF components, and video amplifiers, requiring only IF input and video output connections and DC power for operation. Each subsystem is fully calibrated and characterized. This eliminates the usual interfacing and alignment difficulties encountered when assembling a system from individual components.

This data sheet describes three of the most common types of phase detectors. Other configurations are available on special order.

GLOSSARY

RHG is pleased to provide this section to assist professional engineering personnel with some of the new "language" being used in the field.

Angular Accuracy

Angular accuracy is defined as the difference, in degrees, between the actual input phase difference and the phase difference determined from the output voltage using the nominal phase detector transfer function. In these phase detectors, accuracy is guaranteed for phase angles with ± 45° of crossover.

For example:

For cosine output:

$-135° \leq \phi \leq -45°, 45° \leq \phi \leq 135°$

For sine output:

$-180° \leq \phi \leq -135°, -45° \leq \phi \leq 45°,$
$135° \leq \phi \leq 180°$

Ratio Accuracy

On a return to boresight system, the levels and phase polarity of the Δ (difference) inputs relative to the Σ (sum) input, are measured. The accuracy is defined as how closely the system can detect crossover, i.e., zero Δ level. This accuracy is stated as the highest ration of Δ/Σ that will produce a zero output voltage.

Settling Time

Settling time is the time required for the phase detector output to stabilize within rated accuracy limits, for a pulsed IF input.

Dynamic Range

The phase detector is guaranteed to be within rated accuracy as long as both input levels are within the specified dynamic range, and as long as the difference in input levels is no greater than 30 dB.

Information Bandwidth

The information bandwidth is the subsystem 3 dB IF bandwidth (referred to the input). The video bandwidth is amply wide to be transparent to the information bandwidth.

Accuracy Bandwidth

The accuracy bandwidth is the range of center frequencies over which rated accuracy is maintained. This is the necessity less than the Information Bandwidth.

DISTRIBUTION

	No. of Copies
Defense Documentation Center Cameron Station Alexandria, Virginia 22314	12
IIT Research Institute ATTN: GACIAC 10 West 35th Street Chicago, Illinois 60616	1
DRSMI-LP, Mr. Voigt	1
DRDMI-T, Dr. Kobler	1
DRDMI-TBD	3
DRDMI-TI (Reference Copy)	1
DRDMI-TI (Record Set)	1

	No. of Copies
DRDMI-T- Mr. Fagan	1
DRDMI-TE- Mr. Lindberg	1
-TE- Mr. Low	1
-TE- Mr. Litton	1
-EA- Mr. Lee	1
DRCOM-HEL-Mr. Otto	1
-Mr. Milton	1
Engineering Experiment Georgia Institute of Technology Atlanta, Georgia 30332 ATTN: Dr. Edward K. Reedy	2
Dr. George W. Ewell	2
Bahelle Durham Office P. O. Box 8796 Dorham North Carolina 27707	1
US Army Materiel Systems Analysis Activity Attn: DRXSY-MP Aberdeen Proving Ground, MD 21005	1

U.S. GOVERNMENT PRINTING OFFICE 1979—640-122/570 REGION NO. 4